Dear **Reviewer #1** and **Reviewer #2,**

We thank you for your constructive comments and suggestions for improving the paper. We considered all comments carefully and reworked the manuscript substantially. Especially the suggestion by Reviewer #1 to validate the paper more carefully with additional datasets lead to major changes of the manuscript. This did not only further improve and confirm the model but it also helped us to shorten the paper significantly, by in total four pages in the final two-column format.

Below we like to list the major changes of the manuscript:

- Five additional datasets from independent CT experiments were added for validation of the model formulation for temperature gradient metamorphism (TGM).
- These added CT data validated and confirmed the TGM formulation of the model and allowed to determined the two free parameters α_1 and A_{min} independently from the radar measured anisotropy time series.
- Because α_1 (for TGM) was determined independently, the other free parameter α_2 (to describe the settling-induced growth of horizontal structures) could be determined from radar data after α_1 has already been fixed by CT data.
- The reduction of the solution space of the free parameters from two dimensions (α_1, α_2) to a single dimension (α_2) and a slight correction of the radiation data allowed for determination of the free parameter α_2 simply by minimizing the root-mean-square error between model and radar anisotropy time series. This allowed us to remove the entire section about the cost function to determine the free parameters.
- Because the two parameters α_1 and α_2 are now determined independently, several paragraphs which previously discussed their relation could be removed.
- To avoid confusion we like to note here that the definitions of α_1 and α_2 have been swapped compared to the initially submitted TCD manuscript.
- Additionally, we combined the two sections *Data sets and testsite* and *Methods: model forcing and calibration* into a single section *Datasets and methods* which improved the flow of the paper and helped to shorten many paragraph.
- The model part about melt metamorphism was removed and is now only suggested as a speculative part in the discussion.
- A section about the model evaluation has been added.
- Two full page figure which previously showed snow temperate and snow height in the Appendix have been moved into the supplementary files.
- We carefully examined references to previously published work to avoid any mis- or over-interpretation and describe now more clearly how we interpret their work.
- Care was taken to clearly identify what is an assumption or hypothesis.

Additionally to these major changes, we considered all minor comments and suggestions of the Reviewer. The answers to these comments can be already found in the interactive discussion forum:

- https://www.the-cryosphere-discuss.net/tc-2019-63/#discussion

Because the manuscript was reworked substantially we think that it would not help the Reviewers to upload a track-change version. In case this is required for formal reasons or requested by the Reviewers we would definitely provide such a document.

With best regards, the authors

S. Leinss, H. Löwe et al.

Modeling the Evolution of the Structural Anisotropy of Snow

Silvan Leinss[1], **Henning Löwe**[2], **Martin Proksch**[2], **and Anna Kontu**[3]

[1]Institute of Environmental Engineering, Swiss Federal Institute of Technology in Zurich (ETH), Zürich, Switzerland
[2]Institute for Snow and Avalanche Research SLF, Davos, Switzerland.
[3]Finnish Meteorological Institute FMI, Arctic Research, Sodankylä, Finland.

Correspondence: S. Leinss (leinss@ifu.baug.ethz.ch)

Abstract. The structural anisotropy of snow ~~that originates from a~~ characterizes the spatially anisotropic distribution of the ice ~~matrix and the pore space,~~ and air microstructure and is a key ~~quantity to understand physical snow propertiesand to improve their parameterizations. To this end~~ parameter for improving parameterizations of physical properties. To enable the use of the anisotropy in snowpack models as internal variable, we propose a ~~minimal empirical model to describe~~ simple model based on a rate-equation for the temporal evolution~~of the structural anisotropy and publish the extensive, calibration dataset consisting of meteorological, radar, and micro computer~~ . The model is validated with a comprehensive set of anisotropy profiles and time-series from X-ray tomography (CT) ~~data. The dataset was acquired near the town of Sodankyläin Northern Finland. The model is tailored to immediate implementation into common snow pack models driven by meteorological data as its parametrization is solely based on macroscopic, thermodynamic fields. Here we use output data of the physical model SNOWPACK to drive our model. The model implements rate equations for each snow layer and accounts for snow settling and~~ and radar measurements. The model includes two effects, namely temperature gradient metamorphism ~~, which are taken to be the main drivers of the temporal evolution of the structural anisotropy. The model is calibrated with available time series of anisotropy measurements spanning four different winter seasons. The calibration measurements were obtained from polarimetric radar data which were analyzed with respect to the dielectric anisotropy of snow. From the detailed comparison between simulated anisotropy and radar time series we identify settling as the main mechanism causing horizontal structures in the snow pack. The comparison also confirms temperature gradient metamorphism as the main mechanism for vertical structures . For validation of the model we use~~ and settling, and can be forced by any snowpack model that predicts temperature and density. First, we use CT time-series from lab experiments to validate the proposed effect of temperature gradient metamorphism. Next, we use SNOWPACK simulations to calibrate the model against radar time-series from the NOSREX campaigns in Sodankylä, Finland. Finally we compare the simulated anisotropy profiles against field-measured full-depth ~~profiles of anisotropy measurements obtained from CT data. The results show that the model can predict the measured CT profiles quite accurately. For depth hoar, differences between modeled anisotropy and the anisotropy derived from exponential correlation lengths are observed and discussed in view of potential limitations.~~ CT profiles. Our results confirm that the creation of vertical structures is mainly controlled by the vertical water vapor flux. Our results further indicate a yet undocumented effect of settling on the creation of horizontal structures. Overall the model is able to reproduce the characteristic anisotropy variations in time series of 4 different winter seasons with a very limited set of calibration parameters.

1 Introduction

Deposited snow is a porous material that continuously undergoes microstructural changes in response to the external, thermodynamic forcing imposed by the atmosphere and the underlying soil. In some cases, the microstructure can develop a significant structural anisotropy, i.e. the non-spherical ice particles develop a preferential orientation, often in the vertical or horizontal direction. Among other microstructural properties, a significant amount of work was recently dedicated to understand the impact of the structural anisotropy which is a key parameter to improve predictions

of different snow properties like the thermal conductivity (Izumi and Huzioka, 1975; Calonne et al., 2011; Shertzer and Adams, 2011; Riche and Schneebeli, 2013; Calonne et al., 2014), mechanical (Srivastava et al., 2010, 2016; Wiese and Schneebeli, 2017), diffusive and permeable properties (Zermatten et al., 2011; Calonne et al., 2012, 2014), ~~and also~~ as well as the electromagnetic permittivity (Leinss et al., 2016, and references therein). Especially the thermal conductivity shows a strong dependence on the structural anisotropy (Löwe et al., 2013; Calonne et al., 2014). Depending on snow type, the thermal conductivity can vary by an order of magnitude at a given density: this variability is discussed with respect to the ~~limits of a completely horizontally and completely vertically structured snow pack~~ theoretical limits defined by a microstructure of either vertical or horizontal series of ice plates (Sturm et al., 1997).

The ~~anisotropy of the snow microstructure~~ structural anisotropy is commonly characterized by different variants of geometrical or structural fabric tensors. These can be computed e.g. from mean intercept lengths (Srivastava et al., 2016), contact orientations (Shertzer and Adams, 2011), surface normals (Riche et al., 2013) or other second-order orientation tensors that can be constructed from the two-point correlation function of a two phase medium (Torquato and Lado, 1991; Torquato, 2002). The correlation functions can be evaluated in terms of directional correlation lengths which define characteristic length scales of the microstructure (e.g. Vallese and Kong, 1981; Mätzler, 1997; Löwe et al., 2013) and from which the anisotropy can be derived. For snow, the microstructure can be obtained by stereology (e.g. Alley, 1987; Mätzler, 2002) or from computer tomography, CT (Schneebeli and Sokratov, 2004).

However the inclusion of the structural anisotropy in current ~~snow pack~~ snowpack models is still missing due to i) the lack of a prognostic model for the ~~time evolution of the anisotropy~~ anisotropy evolution and ii) the lack of in-situ data for validation. Motivated by recent progress of anisotropy measurements using radar (Leinss et al., 2016) as a solution for ii) it is the aim of the present paper to overcome i) and to suggest a minimal, dynamical model tailored to direct use in common, operational ~~snow pack models. The model acts also as a link to connect spatially depth-averaged but temporally high-resolution anisotropy time series from radar with the spatially high-resolution but temporally sparse computer tomography measurements.~~ snowpack models.

The model ~~presented in this paper~~ is based on a simple rate equation which ~~mainly accounts for the influence of snow settling and~~ incorporates temperature gradient metamorphism and snow settling. Each contribution is formulated in terms of ~~macroscopic physical variables like strain rate, temperature and temperature gradient .~~ common, macroscopic state variables (temperature, temperature gradient and strain rate) which are provided by detailed snowpack models like SNOWPACK (Bartelt and Lehning, 2002; Lehning et al., 2002a, b) , CROCUS (Brun et al., 1989, 1992) or SNTHERM (Jordan, 1991). The magnitude of each contribution is controlled by ~~a free parameter~~ free parameters which we calibrated with ~~the radar measurements published in (Leinss et al., 2016). The calibration dataconsists of radar-measured anisotropy time series covering~~ laboratory CT data, literature data, and radar time series of the anisotropy evolution over four winter seasons between ~~October~~ Oct 2009 and May ~~2013.~~

~~The input of our model is based on common state variables provided by detailed snow pack models like SNOWPACK Bartelt and Lehning (2002); Lehning et al. (2002a, b) , CROCUS (Brun et al., 1989, 1992) or SNTHERM (Jordan, 1991). Here we used SNOWPACK.~~ 2013 with 4 hour resolution. The model links temporally high-resolution but vertically averaged anisotropy time series from radar with vertically high-resolution but temporally sparse CT measurements and is validated against field-measured, full-depth CT anisotropy profiles.

The paper is structured as follows: Section 2 discusses relevant processes which influence the structural anisotropy and casts them into rate equations. Section 3 presents ~~the test site and specifies the field measurement. Section 3.0.1 explains the forcingand calibration of the model SNOWPACK and the calibration of the~~ experimental data and their integration for model forcing, calibration and validation. Section 4 validates the influence of TGM on the modeled anisotropy, presents the seasonal evolution of the anisotropy ~~model. Section 4 presents the results of the simulated anisotropy profiles and compares them with computer tomographic data~~according to the full model and validates these results with field-measured CT profiles. Section 5 discusses capabilities and deficits of the model and ~~indicates possible uncertainties for~~ of anisotropy measurements. Section 6 concludes the paper and ~~Section 7 lists used data sets and their~~ Sect. 7 lists the data availability. The Appendix details the preprocessing of meteorological data and the calibration of SNOWPACK.

Supplementary files provide additional figures about the processing work flow, ~~internal snow temperatures,~~ meteorological data, radiation balance, ~~analysis of SNOWPACK model variants, cost functions for model calibration,~~ density, SSA and correlation lengths derived from CT data, analysis of SNOWPACK model variants, visualizations of snow properties~~(from SNOWPACK) and additional anisotropy simulations~~, and results of anisotropy model variants.

2 A dynamical model for the structural anisotropy

2.1 ~~Preliminaries~~Definition of the anisotropy

For quantifying the structural anisotropy, we follow the definition in ~~Leinss et al. (2016)~~ (Leinss et al., 2016) and use the normalized difference of a characteristic horizontal length scale a_x and a vertical length scale a_z~~and define the~~

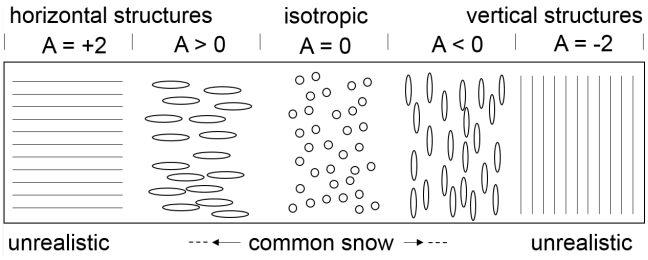

Figure 1. ~~Structural anisotropy of different~~ Different structures and their anisotropy according to ~~definition~~ Eq. (1). Snow has only a small anisotropy and never reaches the unrealistic cases of horizontal planes or vertical needles.

~~anisotropy as~~ :

$$A = \frac{a_x - a_z}{\frac{1}{2}(a_x + a_z)}. \tag{1}$$

Different characteristic length scales can be chosen. Commonly ~~, the~~ exponential correlation lengths $a_i = p_{\mathrm{ex},i}$ are used as defined in (Mätzler, 2002)~~are used~~. According to Eq. (1), the structural anisotropy ranges from ~~$A = -2$~~ -2 (vertical needles) to ~~$A = +2$~~ +2 (horizontal planes) with $A = 0$ for randomly shaped or spherical particles (~~visualized in~~ Fig. 1). As detailed in ~~Leinss et al. (2016), the use of~~ (Leinss et al., 2016), a normalized difference is convenient ~~,~~ compared to the ~~anisotropy definition defined~~ definition via an aspect ratio ~~,~~ ($A' = a_z/a_x$~~, because averaging equally positive and negative values of A result here in isotropy with~~) because equally prolate and oblate particles with interchanged semi-axis have then the same magnitude for the anisotropy and averaging them results in isotropy ($A = 0$). The normalized difference ~~defined in Eq.~~ and the frequently used grain size aspect ratio A' are ~~related by~~ however equivalent and can be related by

$$A' = \frac{2 - A}{2 + A} \quad \text{or equivalently} \quad A = 2\frac{1 - A'}{1 + A'} \quad \text{or equivalently} \quad A = \frac{2 - A'}{2 + A'} \tag{2}$$

This relation is helpful ~~to compare the anisotropy values of this paper with anisotropy valuesfrom other publications which are often given by the aspect ratio A'. For weak anisotropies this relation can be approximated as $A' \approx 1 - A$. For~~ for a comparison with literature values. For snow a common range is $A' \approx 0.75...1.3$ but larger values up to 1.4 might occur (Alley, 1987; Davis and Dozier, 1989; Schneebeli and Sokratov, 2004; Fujita et al., 2009; Calonne et al., 2014). In this range, equally to $A \approx +0.3... - 0.3$, the ~~difference $|(1 - A) - A'|$ is~~ approximation in Eq. (2) deviates less then 5% from A' with respect to A'.

For ~~definiteness~~conciseness, we refer to "horizontal structures" when the horizontal length scales are larger then the vertical ~~scale~~ones, $a_x, a_y > a_z$, hence $A > 0$. Accordingly, "vertical structures" describe snow with larger vertical length scales than horizontal ones, $a_z > a_x, a_y$~~such that~~ , equivalent to $A < 0$.

2.2 Evolution of the anisotropy

Quite generally, the anisotropy ~~A in seasonal snow~~ evolves from horizontal structures in ~~fresh~~ new snow, over ~~rather~~ isotropic structures in decomposing rounded grains, to vertical structures under the influence of temperature gradient metamorphism (Schneebeli and Sokratov, 2004; Calonne et al., 2014) and ~~, at a late stage, returns to isotropy from~~ might return to isotropy during melt processes. To describe this evolution we assume the following rate equation

$$\frac{\partial}{\partial t} A(z,t) = \underline{_{\mathrm{strain}}(z,t) +} \dot{A}_{\mathrm{TGM}}(z,t) + \underline{A_{\mathrm{melt}}} \dot{A}_{\mathrm{strain}}(z,t) \tag{3}$$

The first term ~~$\dot{A}_{\mathrm{strain}}(z,t)$~~ accounts for the ~~formation of horizontal~~ growth of vertical structures due to ~~microscopic grain rearrangement in snow under settling~~temperature gradient metamorphism (TGM), the most common type of snow metamorphism. The second term ~~, $\dot{A}_{\mathrm{TGM}}(z,t)$,~~ accounts for the ~~growth of vertical~~ formation of horizontal structures due to ~~temperature gradient metamorphism (TGM) . The third term, $\dot{A}_{\mathrm{melt}}(z,t)$, causes~~ microscopic grain rearrangement causing the settling (strain) of snow. Further terms could be added to account e.g. for a possible rounding of grains ~~and a decay of the anisotropy due to~~ by melt metamorphism. ~~Naturally, in snow all these processes are coupled, so our choice is a pragmatic approximation that seeks~~ For simplicity we start with the assumption of an additive decomposition ~~in terms~~ of these processes, though naturally, all these processes are coupled (e.g., Wiese and Schneebeli, 2017).

As common for snow models focusing on the evolution of microstructural properties of individual snow layers (Bartelt and Lehning, 2002), we describe the anisotropy evolution in each layer with a Lagrangian viewpoint where the reference frame is attached to a material element. Therefore we drop the z-dependence in Eq. (3)~~which would be required for an Eulerian description where snow layers "sink" through the reference frame fixed in space~~. Further, we restrict our model to flat terrain and do not consider any forces acting parallel to the snow layers (in the x- or y-direction). This implies that gravity and temperature gradient are strictly applied in the z-direction.

2.3 ~~Gravitational settling~~

~~The first term in Eq. , $\dot{A}_{\mathrm{strain}}(t)$, accounts for gravitational settling and densification of snow which apparently creates horizontal structures which can be observed in polarimetric radar data (Leinss et al., 2014, 2016) as well as in computer tomographic data (Wiese and Schneebeli, 2017) . Densification, in contrast to isotropic contraction by a~~

~~sintering stress, was shown to be an anisotropic process: gravity causes an uniaxial squeeze of the snow structure in the z-direction (Fig. 3 and 4 in Schleef and Löwe, 2013) which increases A. The ice matrix is squeezed such that the air pores are filled with above situated ice grains which move into the gaps by compaction (Theile et al., 2011; Löwe et al., 2011; Schleef and Löwe, 2013) , possibly complemented by rotation of individual fragments of the ice matrix (Löwe et al., 2011), and possibly also by falling of above situated ice grains into the air-filled gaps (Vetter et al., 2010). In the absence of detailed quantitative work about the anisotropy of this process we start with the simplest assumption of an affine deformation where all length scales of the structure inherit the macroscopically imposed scale change from strain. In this case the strain rate and the vertical correlation lengths are related by $\dot{\epsilon}(t) = \dot{a}_z/a_z$. However, because of the heterogeneous microstructure of snow the assumption of an affine deformation needs to be mitigated. To account for non-affine effects we introduce an empirical correction factor α_1 and hence proceed with~~

$$\dot{\epsilon}(t) = \frac{1}{\alpha_1}\frac{\dot{a}_z(t)}{a_z(t)}.$$

~~Then, the anisotropy change rate $\dot{A}(t)$ caused by a strain-induced shortening of the correlation length a_z can be expressed as~~

$$\dot{A}(t)_{\text{strain}} = \frac{\mathrm{d}}{\mathrm{d}t}A\big(a_z(t), a_x\big) = \left(\frac{\partial A}{\partial a_z}\right)\dot{a}_z(t).$$

~~Using Eq. and this can be rewritten as~~

$$\dot{A}_{\text{strain}}(t) = \alpha_1\dot{\epsilon}(t)\left(\frac{A^2}{4} - 1\right).$$

~~For large $|A| \to 2$ the term $A^2/4 - 1$ approaches zero and ensures that the anisotropy cannot grow beyond the two extreme values of $A = \pm 2$, even for very large strain rates. However, because the compression of snow is not an affine compression it is unrealistic that large values of A are reached. Therefore, we modify this term and introduce an empirical upper threshold for the anisotropy, $A_{\max} \approx 0.30$, which is based on the maximally observed values for horizontal anisotropies in literature (Leinss et al., 2016; Wiese and Schneebeli, 2017). For negative values of A, no modification is applied. This leads to~~

$$\dot{A}_{\text{strain}}(t) = \alpha_1\dot{\epsilon}(t)\begin{cases}\left(\frac{A^2}{4} - 1\right) & A \le 0.\\ \left(\frac{A^2}{A^2_{\max}} - 1\right) & A > 0.\end{cases}$$

~~The strain rate, $\dot{\epsilon} < 0$, ranges between $\dot{\epsilon} \approx -10^{-4}\,\mathrm{s}^{-1}$ for fresh snow with a very low density to $\dot{\epsilon} \approx -10^{-7}\,\mathrm{s}^{-1}$ for old snow of high density (Bartelt and Lehning, 2002). Both, the strain rate $\dot{\epsilon}$ and the A^2 -terms are always negative, therefore snow settling alway increases the anisotropy A.~~

2.3 Temperature gradient metamorphism

~~The second term in Eq. , $\dot{A}_{\text{TGM}}(t)$, accounts for temperature gradient metamorphism (TGM), the most common type of snow metamorphism. Yosida (1955) showed that TGM causes an anisotropic growth of ice crystals which~~

For TGM ice crystals preferably grow into the opposite direction of the heat- and water vapor flux, for both, ~~a horizontal and a~~ an applied horizontal or vertical heat flux (Yosida, 1955, p. 52–56). The ~~water vapor flux J_{V} is mediated by diffusion which is driven by a water vapor pressure gradient induced by a temperature gradient. In winter, commonly the soil below the snow pack is warmer than the atmosphere. Therefore, the water vapor pressure is higher at the bottom of the snow pack compared to the cold snow surface. Thus, water molecules diffuse from the bottom up through the ice matrix and form a vertical water vapor flux. Water molecules accumulate on crystals which have a colder temperature than the surrounding air (the bottom side of crystals) and sublimate on the warmer (upper) side of the crystals. This local temperature difference with respect to the surrounding air originates from the higher thermal conductivity of ice which distributes heat faster over the crystal volume. The resulting water transport mechanism has been~~ underlying water transport mechanism, mediated by a vapor flux from ice grain to ice grain, is often termed "hand-to-hand" transport as suggested by Yosida (1955, p. 31–34). ~~With computer tomography,~~ Pinzer et al. (2012) confirmed this mechanism ~~and revealed further details: the hand-to-hand transport causes an apparent advection of the ice matrix caused by the downwards motion of (air/ice and ice/air) interfaces that advance by growth or sublimation in the opposite direction of the vapor flux. This leads to~~ and demonstrated a rapid reorganization of the ice matrix ~~with concurrently growing crystals. Pinzer et al. (2012) observed a residence time of water molecules in the ice phase of only few dayswhich makes the idea of~~ within a few days. The rapid reorganization renders the perception of a slowly growing ice ~~grains somewhat confusing as *only the "memory" of the grain, encoded in the temporal correlation of the structure, survives* (Pinzer et al., 2012). This continuous reordering of the ice structureunder persistent temperature gradients leads to a higher chance for~~ grain misleading as "only the 'memory' of the grain, encoded in the temporal correlation of the structure, survives" (Pinzer et al., 2012) . Thereby, large vertical structures ~~to survive (depth hoar chains)~~ have a higher chance to survive while small structures quickly disappear. ~~To mimick~~

To mimic this structural reorganization~~of the ice matrix~~, we model the growth of vertical structures proportional to the magnitude of the water vapor mass flux: $\dot{A}_{\text{TGM}} \propto |J_{\text{V}}|$.

~~The~~ We use the absolute value $|J_{\text{v}}|$~~is used because vertical structures can grow independent on the sign of J_{v}. In seasonal snow the~~ , because the anisotropy does not contain

any information about the growth direction but only about the growth orientation.

In winter, the vapor flux direction is usually positive (upwards) but can be ~~negative~~ reverse in spring, when the ~~(eventually melting)~~ eventually melting snow surface is warmer than the underlying ~~snow pack, which is likewise the case in perennial snow packs. In contrast, temperature gradients changing their direction~~ snowpack. With strong diurnal cycles, the flux direction can also alternate on a daily ~~scale~~ basis, but apparently these oscillating temperature gradients seem not to ~~increase the anisotropy but cause a rounding of grains (Pinzer and Schneebeli, 2009)~~cause growth of faceted crystals: according to Pinzer and Schneebeli (2009) the morphology of the snow structure evolves slower and "did not show any sign of conventional TGM". Therefore, we exclude the effect of daily alternating temperature gradients ~~on the anisotropy~~ by averaging temperature gradients over 24 hours~~. Larger averaging windows of multiple days did only weakly alter the results. It follows that~~ :

$$\dot{A}_{\mathrm{TGM}} \propto |\langle J_{\mathrm{V}}\rangle_{24\mathrm{h}}|. \tag{4}$$

As indicated in Fig. 1, ~~a perfect needle state has never been observed in a snow pack. Hence we like to restrict the anisotropy to values above a practical minimal anisotropy ,~~ perfect needle microstructures do not exist in reality. Therefore we assume a minimal anisotropy A_{min} ~~, which is possible by TGM. By definition, A_{min} must be larger than -2 (vertical needles). In literature we found that the most negative observed anisotropy values range between $A_{\mathrm{min}} = -0.2$ and $A_{\mathrm{min}} = -0.35$, corresponding to the range $A' = 1.2...1.4$, Eq. , as observed by Fujita et al. (2009): $A' = 1.18$, possibly up to 1.44, Schneebeli and Sokratov (2004): $A' = 1.12$, Alley (1987) : $A' = 1.2$, possibly up to 1.4, Calonne et al. (2014): $A' = 1.25$, and $A = -0.3 \pm 0.1$ (CT results, this paper). Calonne et al. (2014) also showed that the anisotropy converged to the value of about $A' = 1.25$ ($A = -0.22$) within three weeks during a constant temperature gradient of . The observation of a limited growth of anisotropy seems very likely to be related to the limitation of grain size growth as observed by (Sturm and Benson, 1997) for depth hoar crystals. Despite the differences in the definition of anisotropy metrics used in the examples above, it seems reasonable to empirically limit the growth of vertical structures by a threshold that we set to $A_{\mathrm{min}} = -0.30$.~~

~~Additionally, we assume that horizontal structures in fresh snow decay significantly faster than the growth speed of vertical structures in old snow and add~~ that can be practically attained by adding an empirical, quadratic weighting function. ~~A faster decay rate of fresh snow compared to old snow partially compensates the fact that any grain size dependence was neglected in the model: the lifetime of small grains in fresh snow should be significantly shorter than the lifetime of large crystals in old snow .~~

~~With the above~~ This function also amplifies the decay of horizontal structures modeled for new snow which should transform faster because small grains evaporate relatively quickly. The function also slows down the evolution of vertical structures which are modeled for snow which has experienced already strong TGM and has therefore relatively large grains. With these considerations, we model the ~~second term of Eq. proportional to the vertical water vapor mass flux J_v (kg m^{-2} s^{-1}) and the positive prefactor α_2 .~~ growth of vertical structures by

$$\dot{A}_{\mathrm{TGM}}(t) = -\alpha_{\underline{2}1} \frac{|\langle J_{\mathrm{v}}\rangle_{24\mathrm{h}}|}{\rho_{\mathrm{ice}} f_\mu(\cdot)} \cdot \begin{cases} \frac{(A-A_{\mathrm{min}})^2}{A_{\mathrm{min}}^2} & A \geq A_{\mathrm{min}}. \\ 0 & A < A_{\mathrm{min}}. \end{cases} \tag{5}$$

The ~~factor α_2 determines~~ positive prefactor α_1 defines the coupling-strength of the right hand side ~~of Eq. and the growth-rate of vertical structures and is later determined empirically based on measured anisotropy time seriesto~~ the anisotropy change rate that must be determined from experiments. On dimensional grounds, we divided the water vapor flux by the density of ice ρ_{ice} (kg m$^{\underline{3}}$ $^{-3}$) to obtain a velocity. This velocity can be interpreted as the vertical, average ~~ice particle velocity . Divided~~ velocity of water molecules. As the lifetime of evaporating ice particles should depend on their size, we divided by a characteristic ~~length scale~~ microstructural length scale, $f_\mu(\cdot)$ (m)~~of the microstructure results in the average change rate~~ , which leads to the correct units (s^{-1}) of the change rate of the structural anisotropy. ~~We found, that the model best predicts the measured anisotropy evolution by simply setting $f_\mu(\cdot) = 1\,\mathrm{mm}$, constant, instead of considering any grain-size dependence. A more physical approach would be to characterize each grain type and size by its potential velocity to transform into vertical structures by a more sophisticated definition of $f_\mu(\cdot)$. Interestingly, any simple, empirical relation could not produce better results compared to the fixed factor $f_\mu(\cdot) = 1\,\mathrm{mm}$.~~

~~The water vapor~~ The vapor flux is mediated by diffusion which is driven by a water vapor pressure gradient induced by a temperature gradient. Therefore, the vertical water vapor mass flux J_{v} (kg m^{-2} s^{-1}) ~~is caused by diffusion of water molecules and originates in concentration gradients in the snow pack. It can be derived by standard thermodynamic relations as done e.g. in (Lehning et al., 2002b). The~~ follows from Fick's law applied to the water vapor mass density ~~, ρ_{v}~~ $\rho_{\mathrm{v}}(T)$ (kg m^{-3}):

$$J_{\mathrm{v}}(T, \frac{\partial T}{\partial z}) = -D_{\mathrm{vs}} \frac{\partial \rho_{\mathrm{v}}}{\partial z} = -D_{\mathrm{vs}} \frac{\partial \rho_{\mathrm{v}}(T)}{\partial T} \frac{\partial T}{\partial z} \tag{6}$$

The vapor mass density ρ_{v} is given by the water vapor pressure, $p_{\mathrm{S}}(T)$, ~~and~~ which is supposed to be at the saturation point in the pores between the ice crystals. ~~Vapor mass density and vapor~~ Density and saturation pressure are related

by the equation for ideal gases~~and it follows that~~,

$$\rho_{\mathrm{v}}(T) = p_{\mathrm{S}}(T)/(R_V T), \tag{7}$$

where $R_V = R/M_{\mathrm{w}} = 461\,\mathrm{J\,kg^{-1}\,K^{-1}}$ is the specific gas constant for water vapor, $M_{\mathrm{w}} = 0.018\,\mathrm{kg\,mol^{-1}}$ ~~is~~ the molar mass of water and $R = 8.314\,\mathrm{J\,mol^{-1}\,K^{-1}}$ ~~is~~ the universal gas constant. The ~~water vapor~~ saturation pressure over ice ~~, $p_{\mathrm{S}}(T)$~~ can be well approximated using different formulas (Marti and Mauersberger, 1993) and is given in (Bartelt and Lehning, 2002) by

$$p_{\mathrm{S}}(T) \approx p_{0\mathrm{S}} \cdot \exp\left[L/R_V\left(T_0^{-1} - T^{-1}\right)\right]) \tag{8}$$

with the latent heat of ice sublimation $L = 2.8\,\mathrm{MJ\,kg^{-1}}$ ~~,~~ and the Triple point pressure and temperature of water, $p_{0\mathrm{S}} = 611.73\,\mathrm{Pa}$ ~~, and Triple point temperature $T_0 = 273.16\,\mathrm{K}$ of water~~and $T_0 = 273.16\,\mathrm{K}$.

~~The vertical water vapor mass flux J_{v} is determined by Fick's law applied to the vapor mass density $\rho_{\mathrm{v}}(T)$ and seems to be almost independent on grain size or microstructure (Pinzer et al., 2012, Fig. 11).~~ Because the saturation pressure, Eq. (8), depends only on temperature, ~~the vertical water vapor mass flux~~ Eq. (6) can be written in terms of temperature T and temperature gradient $\frac{\partial T}{\partial z}$ ~~according to (Lehning et al., 2002b):~~ (Lehning et al., 2002b):

$$J_{\mathrm{v}}(T, \frac{\partial T}{\partial z}) = -D_{\mathrm{vs}} \frac{\partial \rho_{\mathrm{v}}}{\partial z} = -D_{\mathrm{vs}} \frac{\partial \rho_{\mathrm{v}}(T)}{\partial T} \frac{\partial T}{\partial z} = -D_{\mathrm{vs}} \cdot \rho_{\mathrm{v}}(T) \cdot \left[\frac{L}{R_{\mathrm{v}} T^2} \frac{1}{T} \frac{\partial T}{\partial z}\right] \tag{9}$$

The effective diffusion constant for water vapor in snow, D_{vs}, is close to the diffusion constant in air, $D_{\mathrm{v,air}} = 2.1 \cdot 10^{-5}\,\mathrm{m^2\,s^{-1}}$ ~~, (Massman, 1998)~~(Massman, 1998), and ranges between 1 and $10 \cdot 10^{-5}\,\mathrm{m^2\,s^{-1}}$ (Sokratov and Maeno, 2000; Colbeck, 1993) ~~, see also~~ and review in (Pinzer et al., 2012). ~~We assumed~~ As the vapor flux seems to be almost independent of grain size or microstructure (Pinzer et al., 2012, Sect. 4.3 and Fig. 11) we assume a constant diffusion constant, $D_{\mathrm{vs}} = 2 \cdot 10^{-5}\,\mathrm{m^2\,s^{-1}}$.

~~Extremely large temperature gradients could naturally occur at the snow surface under extreme conditions but we do not expect that the anisotropy will grow proportionally at such extreme rates. Additionally, extreme temperature gradients could wrongly occur in simulated data. To exclude such temperature gradients, we set a maximum threshold for simulated temperature gradients of $|\Delta T/\delta z| \leq$.~~

2.4 Gravitational settling

2.5 ~~Melt metamorphism~~

~~Despite a lack of calibration data for anisotropy change under melt metamorphism we implement here a simple model. Calibration data is almost not existent, because the radar, which we used to measure the anisotropy evolution and to calibrate our model, cannot penetrate wet snow . Only one event in April 2012 is available where the snow refroze after strong surface melt occurred. Additionally, observational data and models to predict wet snow metamorphism are still rudimentary and except for the model and references in (Lehning et al., 2002a) and (Brun et al., 1992) we could not find any detailed studies. Similar to their given rate equations we model the anisotropy decay due to melt metamorphism as~~

$$\dot{A}_{\mathrm{melt}} = -\alpha_3 A \cdot \theta_{\mathrm{w}}^{\mathrm{v}\,3}$$

Gravitational settling and densification of snow has been assumed to create horizontal structures as indicated by polarimetric radar observations (Leinss et al., 2016). The radar signal did not increase instantaneously with new snow but with a time delay of a few days after snow fall, thereby suggesting a settling effect (Leinss et al., 2016, Sect. 5.4). In the absence of detailed, quantitative work about the anisotropy evolution of new snow we start with the simplest assumption of an affine deformation where all structural length scales inherit the macroscopically imposed strain. Then, the strain rate and the vertical correlation lengths would be related by $\dot{\epsilon}(t) = \dot{a}_z/a_z$. However, because in the heterogeneous microstructure only the air pores can be squeezed while ice particles might build new vertical contact points, an affine deformation needs to be mitigated. ~~To account for~~ For non-affine effects we introduce an empirical correction factor α_2 and hence proceed with

$$\dot{\epsilon}(t) = \frac{1}{\alpha_2} \frac{\dot{a}_z(t)}{a_z(t)}. \tag{10}$$

~~with the empirical constant $\alpha_3 = 2 \cdot 10^{-3}\,\mathrm{day^{-1}}$ and the liquid water volume fraction $\theta_{\mathrm{w}}^{\mathrm{v}}$ in vol.%. The term $\dot{A}_{\mathrm{melt}}$ has always the opposite sign of A and causes therefore always a rounding of grains and a decay of anisotropic structures.~~

Then, the anisotropy change rate $\dot{A}(t)$ caused by a strain-induced shortening of the correlation length a_z can be expressed as

$$\dot{A}(t)_{\mathrm{strain}} = \frac{\mathrm{d}}{\mathrm{d}t} A\left(a_z(t), a_x\right) = \left(\frac{\partial A}{\partial a_z}\right) \dot{a}_z(t). \tag{11}$$

With Eq. (1) and (10) this can be rewritten as

$$\dot{A}_{\mathrm{strain}}(t) = \alpha_2 \dot{\epsilon}(t) \left(\frac{A^2}{4} - 1\right). \tag{12}$$

For large $|A| \to 2$ the term $A^2/4 - 1$ approaches zero and ensures that the anisotropy cannot grow beyond the two extreme values of $A = \pm 2$, even for very large strain rates. However, because compression should increases the vertical contact between ice grains it seems unrealistic that large

values of A can be reached. Therefore, we modify this term and introduce an empirical upper threshold, $A_{\max}$. For negative values of A , no modification is applied. This leads to

$$\dot{A}_{\text{strain}}(t) = \alpha_2 \dot{\epsilon}(t) \begin{cases} \left(\frac{A^2}{4} - 1\right) & A \leq 0. \\ \left(\frac{A^2}{A^2_{\max}} - 1\right) & A > 0. \end{cases} \tag{13}$$

2.5 Initial condition

For the model an initial anisotropy A_{ini} of new snow needs to be specified. The lag between the accumulation of new snow and the anisotropy increase (Leinss et al., 2016, Sect. 5.4) indicates that A_{ini} should be very close to zero, but slightly positive as new snow settles already during accumulation. Furthermore, we think that most non-spherical snow crystals align preferably horizontally by gravity at the time of deposition. This assumption is supported by observations where dendrites were only found with horizontal orientation in artificial snow (Löwe et al., 2011) as well as in natural snow (Mätzler, 1987, Fig. 2.15). To account for initial settling and alignment, chose $A_{\text{ini}} = 0.05$.

2.6 Model behavior and numerical solution

3 ~~Datasets and testsite~~

The model is summarized in (Fig. 2) which shows the anisotropy evolution for different parameters as obtained from the numerical integration of the rate equation using an explicit Euler method (no differences are observed when using Runge-Kutta). Depending on temperature, the time scales of the anisotropy evolution under TGM (Fig. 2a) range between 10 and 300 days because the water vapor flux can vary by 2–3 orders of magnitude (table below Fig. 2). The comparison of the two runs (1) and (1') show that for the same settings negative anisotropies evolve slower than positive anisotropies. The red line (8) shows that even when strong temperature gradients are applied for many years no significant anisotropy change can be observed under conditions used for sample archiving in the lab. Compared to TGM the settling induced anisotropy (Fig. 2b) evolves much faster (hours to days). As both the strain rate $\dot{\epsilon}$ and the A^2 -terms in Eq. (13) are always negative, snow settling always increases the anisotropy. $A_{\min} = -0.7$ and $A_{\max} = 0.3$ indicate the chosen upper and lower limit for the anisotropy.

~~All data for model~~

3 Datasets and methods

A comprehensive set of laboratory and field data was used to calibrate, drive and evaluate the model. Here, we describe the different datasets and the forcing, calibration and

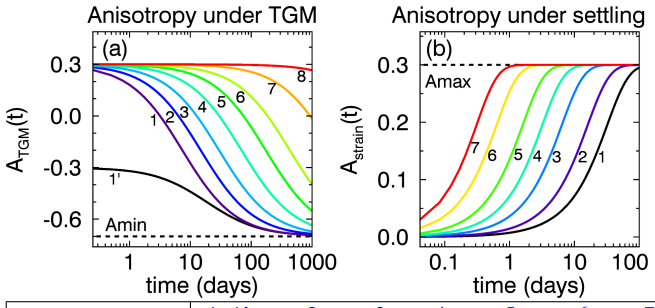

labels in (a)	1, 1'	2	3	4	5	6	7
T (°C)	0	0	0	-20	-20	-40	-40
∇T (K/m)	100	50	25	50	20	50	10
J_v (*)	75	38	19	8.1	3.2	1.3	0.3

labels in (b)	1	2	3	4	5	6	7
$\dot{\epsilon}$ (-10^{-6} s^{-1})	0.05	0.1	0.25	0.5	1.0	2.5	5.0

Figure 2. ~~Picture of~~ Modeled anisotropy evolution for TGM with $\alpha_1 = 0.93$ and settling with $\alpha_2 = 1.68$ for the ~~intensive observation area~~ different tabled conditions (~~IOA~~1-7)~~where field-, radar-, and most meteorological data were acquired~~. ~~Abbreviations are explained in Table 2. Anisotropy validation profiles were extracted at the locations CT-1~~In (a), ~~CT-2a/b, CT-3,~~ 1 and ~~CT-4. The tower-based SnowScat instrument measured~~ 1' differ only by the ~~depth-averaged~~ initial anisotropy~~every four hours over the area "sector 1" (Leinss et al., 2016)~~. ~~It also measured snow water equivalent~~ The red line (~~SWE~~8) ~~in combination with the gamma water instrument, GWI (Leinss et al., 2015). Additional meteorological data were measured at the meteorological mast east of the IOA~~ corresponds to $\nabla T = 100\,\mathrm{K/m}$ and ~~at the automatic weather station~~ $T = -80$ °C. (~~AWS~~*) ~~north~~ The vapor flux J_v is given in units of ~~the IOA~~10^{-8} kg m^{-1} s^{-1} .

~~validation were acquired~~ evaluation of a large ensemble of SNOWPACK runs.

Except for an independent set of laboratory CT data, all field data were acquired in northern Finland 5 km south of the town of Sodankylä at or close to the test site "intensive observation area" (IOA)~~, located south of the town of Sodankyläin northern Finland~~. The IOA is shown in Fig. 3. Table 2 lists all ~~used~~ measurements, sensors and their locations. The measurements were supported by the Nordic Snow Radar Experiment NoSREx-I to -III (Lemmetyinen et al., 2013, 2016).

~~The anisotropy model was forced by depth-resolved snow properties simulated by the model SNOWPACK (v. 3.4.5) . SNOWPACK was driven by meteorological data mainly from the IOA. Precipitation and wind velocity were measured north of the IOA at the automatic weather station (AWS). The radiation balance was measured close to the AWS at the sounding station (short wave)~~

At the IOA, snow pit measurements were performed on a weekly basis. The measurements include snow temperature

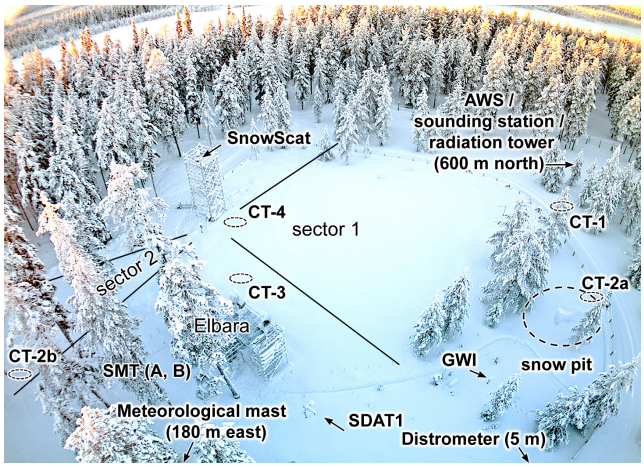

Figure 3. All field-, radar-, and most meteorological data were acquired at the intensive observation area (IOA). The remaining meteorological data were measured at the meteorological mast 180 m east of the IOA and at the automatic weather station (AWS) 600 m north of the IOA. Anisotropy validation profiles were extracted at the locations CT-1, CT-2a/b, CT-3, and CT-4. The depth-averaged anisotropy for "sector 1" was measured every 4 hours with tower-based radar (SnowScat) which also measured the snow water equivalent in combination with the gamma water instrument, GWI (Leinss et al., 2015). Sensor abbreviations are explained in Table 2.

and snow classification. In addition near-infrared (NIR) images of the snow structure were taken on selected dates. For each NIR image we calculated the ratio to a reference image of a Styrofoam panel. The ratio images were used to cross-check CT data, snow type classification and for interpretation of the modeled results.

3.1 Anisotropy determined by computer tomography

For validation of the model we used anisotropy data derived from 3D scans of snow samples analyzed by micro computed tomography (CT). Our analysis includes published data of time series acquired during temperature gradient metamorphism experiments in the lab and snow samples taken in the field during the NoSREx campaign.

The field samples were casted using Diethyl-Phthalate (DEP) for transportation as described in (Heggli et al., 2009) and scanned with a nominal resolution (voxel size) ranging between 10 μ m and ~~at the radiation tower (long wave)~~ 20 μ m. The resulting 3D-gray-scale images were filtered using a Gaussian filter (sigma = 1.2 voxel length, total filter kernel width = 4 voxel lengths). The smoothed images were then segmented into binary ice/air images. For segmentation, an intensity threshold was chosen at the minimum between the DEP peak and the ice peak in the histograms of the gray-scale images.

~~SNOWPACK was calibrated by snow height (IOA, AWS, meteorological mast)and by snow temperature. Snow temperature was measured at the meteorological mast, east of the IOA, with an array of horizontal temperature sensors spaced vertically in the snow pack (Fig. 4).~~ Two-point correlation functions were calculated from the binary images for each direction (Löwe et al., 2013). Then, the correlation lengths, $p_{\mathrm{ex},x}$, $p_{\mathrm{ex},y}$, and $p_{\mathrm{ex},z}$ were derived as described in (Mätzler, 2002). Because of the symmetry in the x -y -plane, the lengths $p_{\mathrm{ex},x}$ and $p_{\mathrm{ex},y}$ were averaged and the corresponding CT anisotropy follows analogue to Eq. (1):

$$A^{\mathrm{CT}} = \frac{0.5(p_{\mathrm{ex},x} + p_{\mathrm{ex},y}) - p_{\mathrm{ex},z}}{\frac{1}{2}\left[0.5(p_{\mathrm{ex},x} + p_{\mathrm{ex},y}) + p_{\mathrm{ex},z}\right]}. \tag{14}$$

~~Free parameters of the model ($\alpha_1, \alpha_2, \alpha_3$, A_{ini}) were estimated by radar-measured time series of depth-averaged anisotropy measurements. The measurements are described in detail in (Leinss et al., 2016) and are based on polarimetric phase measurements from which we derived the dielectric birefringence of~~ To validate the anisotropy evolution under TGM and to determine the free parameter α_1 we used the laboratory data listed in Table 1. The samples TGM-17 (Kaempfer et al., 2005), TGM-2 (Löwe et al., 2013), DH-1 and DH-2 (Riche et al., 2013) were analyzed for their exponential correlation lengths in (Löwe et al., 2013). In addition we used digitized data of the sample C-1 analyzed by Calonne et al. (2014).

Table 1. List of snow samples from laboratory TGM experiments with temperature, temperature gradient, initial ice volume fraction, initial snow type and sub-type, SSA, and duration of the experiment. The corresponding anisotropy evolution is shown in Fig. 5.

sample	T °C	∇T K/m	$f_v(0)$ -	type -	SSA $m^2\,kg^{-1}$	Δt days
TGM-2	-10	100	0.22	DFdc	29.0	11.7
TGM-17	-8	50	0.33	RGsr	21.7	16.0
DH-1	-20	50	0.19	DFdc	22.1	87.5
DH-2	-20	50	0.29	DFbk	20.0	80.5
C-1	-4	43	0.35	RG	20.8	27.7

For validation of the full model with field-measured conditions, almost complete vertical snow profiles were extracted in Finland and preserved for later analysis in Switzerland. Five profiles named CT-1, CT-2a/2b, CT-3, and CT-4, were sampled at the locations shown in Fig. 3 on the ~~snow pack at microwave frequencies. The measurements were done with the SnowScat radar instrument which~~ dates listed in Table 2. The structural anisotropy was determined with a vertical resolution of 1–2 mm. The profiles contain some gaps of a few cm where the samples were not overlapping or sample taking was not possible due to very soft new snow (CT-4), ice crusts or large fragile depth hoar crystals (CT-1). Data of the profiles CT-2a and 2b were combined. Examples of the analyzed 3D snow structure are shown in (Leinss et al., 2016, Fig. 14 and 15)

. Other derived parameters have already been published in (Proksch et al., 2015).

3.2 Anisotropy determined by polarimetric radar

Depth-averaged anisotropy time series were obtained from polarimetric radar measurements acquired by the ground based radar instrument SnowScat. SnowScat was developed and built to analyze the backscatter intensity of snow between 9.2 and 17.8 GHz ~~(Werner et al., 2010; Lemmetyinen et al., 2016)~~ (Lemmetyinen et al., 2016), ESA ESTEC contract 42000 20716/07/NL/EL (available on request from ESA). ~~Tilting and rotation of the radar antennas allowed for anisotropy measurements at both, different incidence- and different azimuth-angles of sector 1 of the IOA.~~ Technical details of the instrument are given in (Werner et al., 2010).

~~For validation, we compared the modeled anisotropyprofiles with computer tomographic measurements of the snow microstructure. Vertical anisotropy profiles were computed from the microstructure which was sampled during four field visits to the location CT-1, -2~~The method for measuring the depth-averaged anisotropy from radar data is detailed in (Leinss et al., 2016) . Here we briefly outline the method: microwaves with a sufficiently long wavelength penetrate the snowpack with negligible scattering losses and accumulate a signal delay by the refractive index of snow. For snow with a spatially anisotropic microstructure the signal delay depends on the polarization of the electric field. The signal delay difference between two perpendicular to each other polarized radar echoes can then precisely be measured interferometrically by determining the co-polar phase difference, CPD (Leinss et al., 2016). From the CPD, the depth-averaged radar anisotropy, ~~-3, and -4 shown in Fig. 3.~~

~~The~~ $A_{\mathrm{avg}}^{\mathrm{CPD}}$, can be derived when snow depth and density are known.

When this method is applied at sufficiently high frequencies (10–20 GHz) $A_{\mathrm{avg}}^{\mathrm{CPD}}$ can be determined with an accuracy of a few percent. The frequency limits are determined such that the radar penetration depth in snow is sufficiently high (upper limit), the system's phase accuracy is much smaller than the total measured CPD, and the penetration into soil (and polarimetric effects of soil) are negligible (lower limit).

About 3200 anisotropy measurements with a temporal resolution of 4 hours were acquired at the IOA during the four winter seasons 2009–2013. Because microwaves frequencies above 10 GHz have almost no penetration into wet snow, the anisotropy during snow melt could not be measured.

3.3 Anisotropy determined by SNOWPACK

Table 2. List of field data ~~sources~~ for model input, calibration and validation. ~~Sites are given with coordinates~~For each site, ~~below follow~~ sensor abbreviations and full sensor names are given, or data set abbreviation and type of measurements.

Intensive observation area (IOA):	67.36185°
SnowScat	SnowScat instrument, tower-based radar for depth-averaged anisotropy measurements and for snow water equivalent.
GWI	Gamma Water Instrument (SWE measurement by gamma ray absorption)
Distr	Distrometer: precipitation classification and precipitation phase (liquid, solid)
SDAT1	Sensor for snow height and air temperature
SMT A,B	Two sensors for soil moisture (at -2, -10 cm), and for soil temperature (at -2 cm)
CT-no.	Snow profile no.1...4, analyzed by ~~computer~~ CT
CT-1	Profile 1, ~~sampling date:~~ sampled on 03 ~~March~~Mar 2011
CT-2a/b	Profile 2a/b, ~~sampling date:~~ sampled on 21 ~~December~~Dec 2011
CT-3	Profile 3, ~~sampling date:~~ sampled on 01 ~~March~~Mar 2012
CT-4	Profile 4, ~~sampling date:~~ sampled on 28 ~~February~~Feb 2013
Snow pit	~~Snow pit for snow~~ snow classification, density, SWE, grain size, snow temperature (manual measurements)
Meteorological mast (arcmast):	67.36205°
arcsnow	Snow height, air temperature (1 m above ground), snow temperature at 10, 20, ..., 110 cm height
arcsoil	Soil moisture, soil temperature at -5, -10,...-50 cm
~~SDvar~~	~~Snow height variability course (7 x snow height)~~
Automatic weather station (AWS):	67.36662°
	Snow height, air temperature (2 m above ground), wind speed ~~, wind~~ and direction, precipitation, ~~relative~~ humidity
Sounding station (near AWS):	67.36660°
CM11	Kipp&Zonen sensor CM11, 305–2800 nm, incoming ~~short wave (global), ISWR,~~ and outgoing short wave ~~,~~
Radiation tower (near AWS):	67.36664°
CG4	Kipp & Zonen sensor CG4, 4500–42000 nm, incoming ~~long wave radiation, ILWR,~~ and outgoing long wave ra

For comparison of modeled results with radar data and to simulate the depth-resolved anisotropy evolution, we forced the anisotropy model with snow properties simulated by the model SNOWPACK (v. 3.4.5). The model was forced by meteorological and soil data and was calibrated with snow height and snow temperature measurements. The following subsections provide intermediate details of the retrieval, pre-processing, and filtering of ~~the ground~~ these measurements. More details are provided in Appendix A1 and A2. Plots of ~~SNOWPACK~~ input, output and control data of SNOWPACK are provided in the supplementary material.

3.4 ~~Meteorological input data~~

3.3.1 Meteorological data

For ~~definition of~~ the snow-atmosphere boundary conditions, SNOWPACK requires the following meteorological input data: air temperature (TA), soil temperature (TSG), relative humidity (RH), wind speed (VW), wind direction (DW), incoming short wave radiation (ISWR) and/or reflected (outgoing) short wave radiation (OSWR), incoming long wave radiation (ILWR) and/or snow surface temperature (TSS), precipitation (PSUM) and/or snow height (HS) and optionally the precipitation phase (PSUM_PH). For monitoring purposes, up to five internal snow temperature measurements (TS1, ..., TS5) at different heights can be provided for comparison with modeled snow temperatures. Most ~~of these quantities were measured~~ input data were measured redundantly by more than one ~~sensors~~ sensor at the IOA ~~and nearby sites~~ (Table 2). Precipitation and wind velocity were measured at the automatic weather station (AWS), 600 m north of the IOA. The radiation balance was measured close to the AWS at the sounding station and at the radiation tower.

To provide physically correct and consistent conditions, the meteorological data were filtered, combined, and interpolated if gaps could not be filled with equivalent datasets ~~. Preprocessing details of meteorological data are provided in Appendix A1~~(for details see Appendix A1). Plots of both measured raw data and filtered ~~and pre-processed data (SNOWPACK input),~~ SNOWPACK input data are provided in the supplementary figures S3–S10. SNOWPACK additionally filters and ~~pre-processes~~ preprocesses the input data and provides them for control (supplementary figures S11–S14).

3.4 ~~Definition of underlying soil~~

3.3.1 Soil data

For the lower boundary condition, SNOWPACK requires a description of at least one soil layer. To define precisely the temperature of the soil-snow interface we defined a single, 5 cm thin soil layer which lower temperature (TSG) was ~~determined~~ provided by the average of four soil temperature sensors at -5 cm and -10 cm (sensor: arcsoil at meteorological mast) and two measurements at -2 cm depth (sensor: SMT at IOA).

For soil moisture we averaged data from six sensors, two from the meteorological mast (arcsoil: -5 cm, -10 cm) and four from the IOA (SMT: two locations, each at -2 cm and -10 cm). ~~For the definition of soil properties at the start of the simulation we provided soil temperature and moisture~~ Temperature and moisture were provided as the average over one week around the simulation start time (1st of ~~September~~Sept).

Figure 4. Snow temperature was measured ~~at every height by~~ with an array of horizontally oriented temperature sensors at the meteorological mast.

The soil composition is described in (Lemmetyinen et al., 2013) as very fine mineral soil composed of 70% sand, 1% clay and 29% silt. For this mineral soil, we assumed a solid volume fraction of 75% and zero ice fraction in autumn. We estimated a density 1800 kg m^{-3}, a heat conductivity of 1.5 W m^{-1} K^{-1} (from ToolBox (2003a)), and a heat capacity of 1000 J kg^{-1} K^{-1} (from ToolBox (2003b)). A soil albedo of 0.2 was determined from the ratio of incoming and reflected short wave radiation data~~(sensor: CM11 at sounding station).~~.

3.4 ~~Snow temperature~~

3.3.1 Snow temperature data

~~The internal snow temperaturewas measured by~~ Snow temperature, used for SNOWPACK calibration, was measured at the meteorological mast, 180 m east of the IOA, with an array of 11 horizontally oriented temperature sensors located at 10, 20, ..., 110 cm above the ground (Fig. 4).

Unfortunately, for this configuration with all sensors attached to the same support stick, we cannot exclude that some air-filled gaps occurred between the sensor elements. Furthermore, it was reported for another, similar sensor configuration that the sensor configuration interfered with snow accumulation and caused the formation of ~~a pit (~~an up to 30 cm deep ~~)~~ pit in the snow around the sensor. ~~For the sensor used here, such measurement errors~~ Such sensor biases can be detected by comparing the lowest snow temperature (at +10 cm above ground) with the measured soil temperature (see ~~Figs. 16 and 17) . For~~ Fig. S17) because for a deep, well insulating ~~snow pack~~snowpack, both temperatures should not vary more than a few K. Manual snow temperature measurements provide an additional validation source for the sensor array measurements.

3.4 ~~Anisotropy determined by polarimetric radar~~

~~For calibration of the anisotropy model we used depth-averaged anisotropy time series which were obtained from polarimetric radar measurements acquired by the ground based radar instrument SnowScat. The method is described in detail in (Leinss et al., 2016). Below, we briefly summarize the method. For technical details of the instrument see (Werner et al., 2010) and also (Leinss et al., 2015) where the instrument was used to determine the snow water equivalent (SWE) at test site IOA.~~

~~Microwaves with sufficiently long wavelength penetrate the snow pack with negligible scattering losses and accumulate a signal delay due to the refractive index of snow. When the snow pack has a spatially anisotropic structure (i.e. preferably horizontal or vertical structures) and the electric field has horizontal and vertical components, the signal delay depends on polarization. The average anisotropy of the snow pack determined by radar,~~ $A^{\mathrm{CPD}}_{\mathrm{avg}}$ ~~, can therefore be derived from the signal delay difference of two perpendicular to each other polarized radar echoes. This signal delay difference can precisely be measured interferometrically by analyzing the phase difference between the two orthogonally polarized microwaves. This phase difference is called the co-polar phase difference, CPD (Leinss et al., 2016). When this interferometric method is applied at sufficiently high frequencies () it is possible to determine~~ $A^{\mathrm{CPD}}_{\mathrm{avg}}$ ~~with an accuracy of a few percent. The frequency limits are determined such that the radar penetration depth in snow is sufficiently height (upper limit), that the measurable phase accuracy is much smaller than the total CPD, and that penetration into soil (and polarimetric effects of soil) are negligible (lower limit). About 3200 anisotropy measurements with a temporal resolution of were acquired during the four winter seasons 2009–2013. Because microwaves frequencies above have almost no penetration into wet snow, the anisotropy during snow melt could not be measured.~~

3.4 ~~Anisotropy determined by computer tomography~~

~~For validation of different active and passive microwaves experiments conducted during the NoSREx campaigns, snow samples comprising almost complete vertical snow profiles were extracted in the field and conserved for a later analysis by means of micro computer tomography (CT). The profiles contain some gaps of a few cm where the samples were not overlapping or sample taking was not possible due to very soft fresh snow, ice crusts or large fragile depth hoar crystals. The profiles were sampled at the five locations, CT-1, CT-2a, CT-2b, CT-3, and CT-4, shown in Fig. 3. Sampling dates are listed in Table 2. The snow samples were analyzed at the WSL-Institute for Snow and Avalanche Research SLF in Switzerland.~~

~~We analyzed the CT data with respect to the structural anisotropy of snow. Other derived snow parameters have already been published in (Proksch et al., 2015). Here we briefly summarize the methodology of sample preparation and processing of the CT-data: for transportation from Finland to the cold lab at SLF, the snow samples were cast using Diethyl-Phthalate (DEP) as described in (Heggli et al., 2009). In the cold lab, the samples were scanned with a nominal resolution (voxel size) ranging from for new snow to for depth hoar. The resulting 3D-gray-scale images were filtered using a Gaussian filter (sigma = 1 voxel length, total filter kernel width = 5 voxel lengths). The smoothed images were then segmented into binary snow/air images. For segmentation, an intensity threshold was chosen at the minimum between the DEP peak and the ice peak in the histograms of the gray-scale images. From the binary images two-point correlation functions were calculated according to Löwe et al. (2013) for each direction and the corresponding correlation lengths,~~ $p_{\mathrm{ex},x}$ ~~,~~ $p_{\mathrm{ex},y}$ ~~, and~~ $p_{\mathrm{ex},z}$ ~~, were derived as described by Mätzler (2002). Examples of the analyzed snow samples are shown in (Leinss et al., 2016, Fig. 14 and 15).~~

~~The anisotropy determined by computer tomography,~~ A^{CT} ~~, is defined analogue to Eq. . Because of the symmetry in the~~ x ~~-~~ y ~~-plane, the correlation lengths~~ $p_{\mathrm{ex},x}$ ~~and~~ $p_{\mathrm{ex},y}$ ~~were averaged:~~

$$A^{\mathrm{CT}} = \frac{0.5(p_{\mathrm{ex},x} + p_{\mathrm{ex},y}) - p_{\mathrm{ex},z}}{\frac{1}{2}\left[0.5(p_{\mathrm{ex},x} + p_{\mathrm{ex},y}) + p_{\mathrm{ex},z}\right]}.$$

~~In contrast to the depth-averaged radar measurements used for model calibration, the anisotropy,~~ A^{CT} ~~, has a vertical resolution of and allows for validation of the simulated anisotropy profiles.~~

3.4 ~~Snow classification and NIR images~~

~~Datasets of manual snow type classification have been acquired on a weekly basis. In addition for several dates near-infrared (NIR) images of the snow structure are available. For each snow image the ratio relative to a reference image of a Styrofoam panel was calculated. The ratio-images were used to cross-check snow type classification as well as the CT data. They were also considered for interpretation of the simulated results. The images are shown in Fig. 9.~~

4 ~~Methods: model forcing and calibration~~

~~The proposed anisotropy model is designed for immediate implementation into snow pack models which provide the following variables for each layer of snow: snow temperature~~ T ~~, vertical snow temperature gradient~~ $\partial T/\partial z$ ~~, and strain rate~~ $\dot{\varepsilon}$ ~~. The software SNOWPACK (Bartelt and Lehning, 2002; Lehning et al., 2002a, b) provides these parameters but does not consider the structural~~

~~anisotropy of snow. To keep the implementation simple enough, we post-processed the output of SNOWPACK and did not intent to feed the anisotropy back into SNOWPACK.~~

3.1 ~~SNOWPACK: calibration and configuration~~

~~SNOWPACK provides~~

3.0.1 Calibration and configuration

SNOWPACK provides a variety of settings to adjust for the local environment and to configure the simulation. Additionally, the radiation balances required some calibration because it was not directly measured ~~over~~ at the IOA. To best replicate measured snow height and temperatures we run for all four seasons more than 5000 simulations with ~~different settings~~ each time different settings (but keeping the same settings for all four seasons) and graded the accuracy of the simulation results by comparison of simulated snow height and snow temperature with measured snow height and temperature (~~TS1, ..., TS5~~details in Appendix A3). To avoid systematic deviations of SWE or snow density we first run SNOWPACK driven by calibrated precipitation (~~details in~~ Appendix A1). Then, we run the best ~~300~~ 230 simulations again but with enforced snow height~~; for~~ , i.e. SNOWPACK tries to estimate the precipitation which is required to reproduce the measured snow height. For a sanity check we verified the simulated SWE. Table 3 summarizes the most important settings which ~~significantly~~ improved the simulation results ~~. Details about the quantitative comparison of snow height and snow temperature and the definition (grading) of the "best" simulations are described in Appendix A3.~~

~~Most relevant settings for SNOWPACK which provided the best results.SNOW_EROSION TRUEWIND_SCALING_FACTOR 2.0...2.5ATMOSPHERIC_STABILITY NEUTRALTHRESH_RAIN 0.7...1.2C, (or PSUM_PH)ISWR ISWR × 0.65...0.95ILWR ILWR × 0.93...0.97SW_MODE INCOMING, (BOTH)~~

~~Simulation results significantlyimproved by setting SNOW_EROSION = TRUE and WIND_SCALING_FACTOR ≈ 2 . Results also improved by setting ATMOSPHERIC_STABILITY to NEUTRAL.~~ significantly. Little difference was found between a fixed threshold for the precipitation phase (THRESH_RAIN~~, Table 3~~) and estimation of the precipitation phase (PSUM_PH) from distrometer data (Appendix A1). When enforcing snow height, snow height was better predicted but SWE was slightly overestimated when reducing the default value HEIGHT_NEW_ELEM = 0.02.

Tree canopy was not considered (CANOPY = FALSE) because the test site was not covered by trees. Still, surrounding trees could have affected the radiation balance ~~. Radiation data~~ which was calibrated by multiplication with constant factors and selection of the best simulation results. Incoming short wave radiation (ISWR) was ~~multiplied by 0.65...0.95~~ reduced (Table 3) which agrees with the fact that the IOA was partially shadowed by trees but short wave radiation was measured on a tower above the trees. Outgoing short wave radiation (OSWR) was ~~not used but~~ internally estimated by SNOWPACK based on the simulated albedo (SW_MODE = INCOMING instead of BOTH). ~~As expected, the calibration factor for~~ The incoming long wave radiation (ILWR) ~~is close to one because ILWR mainly results from diffuse reflected radiation by cloud cover~~needed only a little reduction. Outgoing long wave radiation was not used by SNOWPACK.

Table 3. Most relevant settings for SNOWPACK which produced the best results.

SNOW_EROSION	= TRUE
WIND_SCALING_FACTOR	= 2.0...2.5
ATMOSPHERIC_STABILITY	= NEUTRAL
THRESH_RAIN	= 0.7...1.2°C, (or PSUM_PH)
ISWR	= ISWR × 0.75...0.93
ILWR	= ILWR × 0.93...0.97
SW_MODE	= INCOMING, (BOTH)

3.1 ~~Calibration of the anisotropy model~~

~~Several free parameters of the model had to be determined.The values of A_{min} and A_{max} have already been defined based on literature values in Sect. 2.4 and 2.3.The initial anisotropy of new snow, A_{ini} , is discussed in Sect. 2.5.The remaining three coupling parameters, which describe the effect of settling (α_1), TGM (α_2), and melt metamorphism (α_3), were determined as follows: α_1 and α_2 were estimated iteratively by minimization of~~

3.0.1 Coupling the anisotropy model to SNOWPACK

The proposed anisotropy model is designed for immediate implementation into snowpack models which provide the following variables for each layer of snow: snow temperature T , vertical snow temperature gradient $\partial T/\partial z$, and strain rate $\dot{\varepsilon}$. SNOWPACK provides these parameters but does not consider the structural anisotropy of snow. To keep the implementation simple enough, we post-processed the output of SNOWPACK and did not intend to feed the anisotropy back into SNOWPACK.

SNOWPACK merges two adjacent snow layers when they have similar properties and when their thickness falls below a certain threshold. To keep track of the ~~error (cost function, Eq. A1) between the modeled time series for the anisotropy $A_{\mathrm{avg}}^{\mathrm{mod}}$ (depth-averaged) and the~~ anisotropy evolution of merged layers, we wrote an algorithm to detect when snow layers get merged. The anisotropy ~~$A_{\mathrm{avg}}^{\mathrm{CPD}}$, measured by radar. For calibration we only used radar measurements which were considered reliable enough, i.e. when the snow was~~

~~deep enough such that the radar measurements showed a standard deviations $\sigma(A_{\mathrm{avg}}^{\mathrm{CPD}}) < 0.05$ and when no wet snow perturbed the transmissive radar measurements. Details about optimization and the cost function are provided in Appendix A4.~~ of a merged layer is defined by the average anisotropy of the two original layers weighted by their thickness.

~~Finally, upon determination of α_1 and α_2 , the parameter α_3 was estimated manually, mainly, by considering the melt-event on 11. April 2012. This melt event occurred simultaneously with snow fall which, in spite of settling, did only marginally increase the radar-measured anisotropy. The melt metamorphism term counteracts here the settling-induces anisotropy increase by modeling rounding of anisotropic ice grains. The parameter α_3 is only weakly constrained by measurements a few days around this event. Unfortunately, during the entire melt period, anisotropy measurements with radar are not possible (Sect. ??).~~

3.1 ~~Model calibration for different snow packs~~

~~To specify the uncertainty for the free parameters α_1 and α_2 we did not only globally evaluate the cost function over all four seasons, but also determined α_1 and α_2 independently for each season. The results of this analysis show whether the parameters α_1 and α_2 must be adjusted for every different snow pack or if they could be universally valid, at least for the four seasons of Finish snow~~Extremely large temperature gradients could naturally occur at the snow surface under extreme conditions but we do not expect that the anisotropy will grow proportionally to such extreme gradients. Extreme temperature gradients could also wrongly occur in simulated data. To exclude such temperature gradients, we set a maximum threshold for simulated temperature gradients of $|\Delta T/\delta z| \leq 200\,\mathrm{K\,m^{-1}}$.

~~Furthermore, the cost function was evaluated~~

3.0.1 Ensemble runs

To consider the uncertainty of different SNOWPACK configurations, we run a sensitivity analysis of the model and determined α_2 for the ensemble of the best ~~300 SNOWPACK simulationswith slightly different configuration settings(~~230 SNOWPACK simulations. Each ensemble member consists of 4 seasons simulated with the same SNOWPACK configuration. For each ensemble member, α_2 was determined once for each season independently and once for all seasons together. The ensemble members differed slightly in the following configuration settings: scaling of radiation balance, rain threshold, wind scaling factor, short wave reflected radiation based on albedo simulation or measurements, precipitation phase estimation~~). However, all 300~~ , and different thresholds for the height of new snow elements. All 230 simulations had the following settings in common: snow height was enforced, neutral atmosphere, snow erosion was allowed. The quality ~~of this ensemble of simulations, assessed by comparison to measured snow height and snow temperature,~~ analysis of corresponding SNOWPACK ensemble is shown in ~~histograms in~~ the supplementary Fig. S19. ~~This sensitivity analysis provides an estimate how sensitive the parameters α_1 and α_2 are with respect to slightly changing snow conditions in different ensemble members.~~

3.1 ~~Initial conditions~~

~~Linking the output of SNOWPACK to our anisotropy model required specification of the initial anisotropy for fresh snow and proper handling for merging of snow layers.~~

~~The anisotropy of fresh snow was set to $A_{\mathrm{ini}} = 0.05$. A_{ini} is expected to be positive but close to zero, as each fresh snow layer has already settled during accumulation. The initial value of 0.05 seems to be realistic in view of a strain rate of of fresh snow during the input data sampling interval of one hour.Furthermore, it is likely that snow flakes align preferably horizontally by gravity at the time of deposition. This assumption is supported by observations where dendrites were only found with horizontal orientation in artificial snow (Löwe et al., 2011) as well as in natural snow (Mätzler, 1987, Fig. 2.15).For the initial anisotropy, we neglected any temperature dependence due to lack of representative data . Stronger cohesion between crystals at temperatures close to zero could lead to a more isotropic structure (but with faster settling) compared to cold temperatures were crystals align according to gravity without being influenced by stronger cohesion forces or settling. A temperature dependence for the shape of snow crystals growing in the atmosphere could also influence the initial anisotropy~~

4 Results

4.1 Validation by laboratory experiments

For validation of the TGM formulation we analyzed the anisotropy time series from the five laboratory CT experiments listed in Table 1. The time series are shown in Fig. 5(a) and also in Fig. 5(b). All experiments indicate that the anisotropy has not reached a stable value at the end of the experiment but would further decrease with time. Extrapolating the curves would probably reach a stable state around $A_{\mathrm{min}} = -0.6 \ldots -0.8$ which indicates that A_{min} must be smaller than the lowest observed value of -0.45. Therefore, we choose an practical minimum threshold of $A_{\mathrm{min}} = -0.7$.

A simple check of anisotropy evolution with respect to the vapor flux dependence can be done when ignoring the limiting factor $(A - A_{\mathrm{min}})^2/A_{\mathrm{min}}^2$ in Eq. (5) and setting $\alpha_1 = 1$. By time integration one obtains

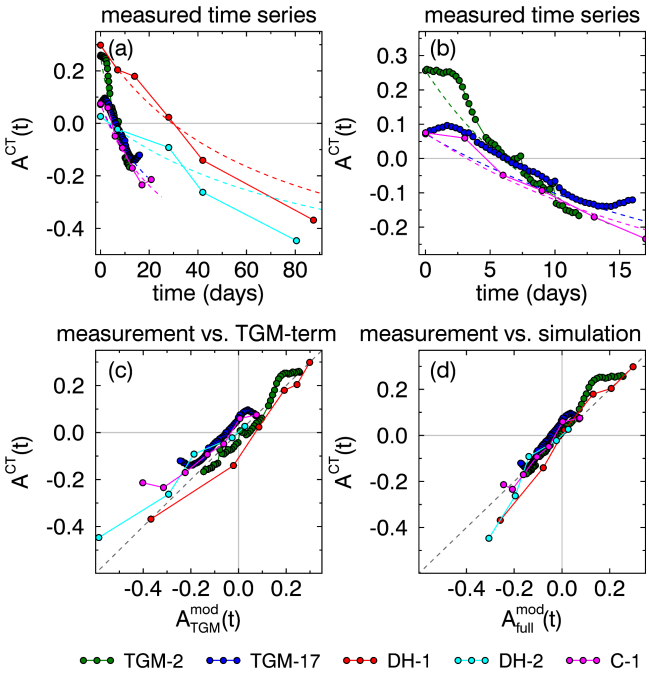

Figure 5. (a): Anisotropy time series $A^{\mathrm{CT}}(t)$ of the laboratory experiments listed in Table 1. Dashed lines indicate modeled results. (b): Zoom into the first 15 days after start of the experiment (c): When ignoring the lower threshold A_{min} and with $\alpha_1 = 1$ the simulated data agrees already well with CT data. (d) With a lower threshold $A_{\mathrm{min}} = -0.7$ and with $\alpha_1 = 0.93$, model and measurements agree even better which indicates that the growth of vertical structures is proportional to the water vapor flux.

$A^{\mathrm{mod}}_{\mathrm{TGM}}(t) = A(0) + |J_{\mathrm{v}}|/(\rho_{\mathrm{ice}} f_\mu) \cdot t$, which agrees well with the experimental data as shown in Fig. 5(c). Because the laboratory CT data was obtained with different temperatures and temperature gradients (listed in Table 1) this proportionality indicates that the growth of vertical structures is almost linearly dependent on the water vapor flux J_{v}.

~~SNOWPACK merges two adjacent snow layers when they have similar properties and when their thickness falls below a certain threshold. To keep track of the anisotropy evolution of merged layers, we wrote an algorithm to detect when snow layers get merged. The anisotropy of a merged layer is defined by the average anisotropy of the two original layers weighted by their thickness~~Then we applied the full TGM term, Eq. (5), including the limiting factor and with $A_{\mathrm{min}} = -0.7$ and determined $\alpha_1 = 0.93$ by minimizing the RMSE (= 0.048) between the laboratory CT data and the simulated data. Figure 5(d) shows the improvements of the results compared to Fig. 5(c).

Above, we have simply set the free microstructural parameter $f_\mu(\cdot)$, which originated from dimensional considerations, to $f_\mu(\cdot) = 1\,\mathrm{mm}$, constant, instead of considering any grain-size dependence in Eq. (5). As the laboratory data agree very well with the simulated data, we think that this is a reasonable approximation.

4.2 ~~Implementation~~

~~The rate equations were solved with a simple explicit Euler method.The classical Runge-Kutta algorithm was also implemented but did not show visible difference to the explicit Euler method which was used for computational efficiency: A single iteration, simulating about 600 000 snow elements takes about (for Runge-Kutta) summing up to about to determine the parameters α_1 and α_2 for a single SNOWPACK ensemble member representing four winter seasons. The entire code was implemented in IDL on a PC with Intel Xeon CPU E3-1270 V2 @ 3.50GHz, 4 cores.~~ An interesting detail appears in Fig. 5(b) at an early stage. The anisotropy seems to be quite stable for a few days and vertical structures start growing not before 2–3 days after start of the experiment.

5 ~~Results~~

4.1 Seasonal evolution of the anisotropy

~~The simulated evolution of the anisotropy is shown in Fig. 6 and Fig. 7. In the upper panels, (a) and (c), the anisotropy of each snow layer is shown in color: yellow and red colors indicate horizontal structures and blue colors indicate vertical structures. The shown profiles are based on input data from the "best" SNOWPACK run, compared to all other ensemble members (Appendix A3). The simulated anisotropy values range approximately between A = -0.2 and A = +0.3. The dates when the CT profiles were obtained in the field are indicated by vertical black dashed lines labeled with CT-1, -2, -3, and -4.~~

~~Below the color-coded depth-resolved profiles, the panels (b) and (d) show time series of the~~ No laboratory data about the anisotropy evolution of new snow is presently available. Therefore, we calibrated the parameter α_2 by run the full model on the output of SNOWPACK and compared the depth-averaged anisotropy measured by radar with the depth-averaged anisotropy ~~. The radar-measured anisotropy~~ of the model results.

The depth-averaged, radar measured anisotropy time series, $A^{\mathrm{CPD}}_{\mathrm{avg}}$, ~~is colored in black, measurements not used for model calibration are shown as gray dots. Red error bars indicate the~~ are shown in the lower panels (b, d) of Figs. 6 and 7 as a line of solid black dots. The corresponding standard deviation of radar measurements acquired with different incidence and azimuth angles ~~. The depth-average of the modeled anisotropy, $A^{\mathrm{mod}}_{\mathrm{avg}}$, is shown in green and gray lines : the green line is the median of the 300 best SNOWPACK runs which~~ of the radar antenna is indicated by red error bars. Radar measurements were considered reliable enough for model calibration when the snowpack was dry and the

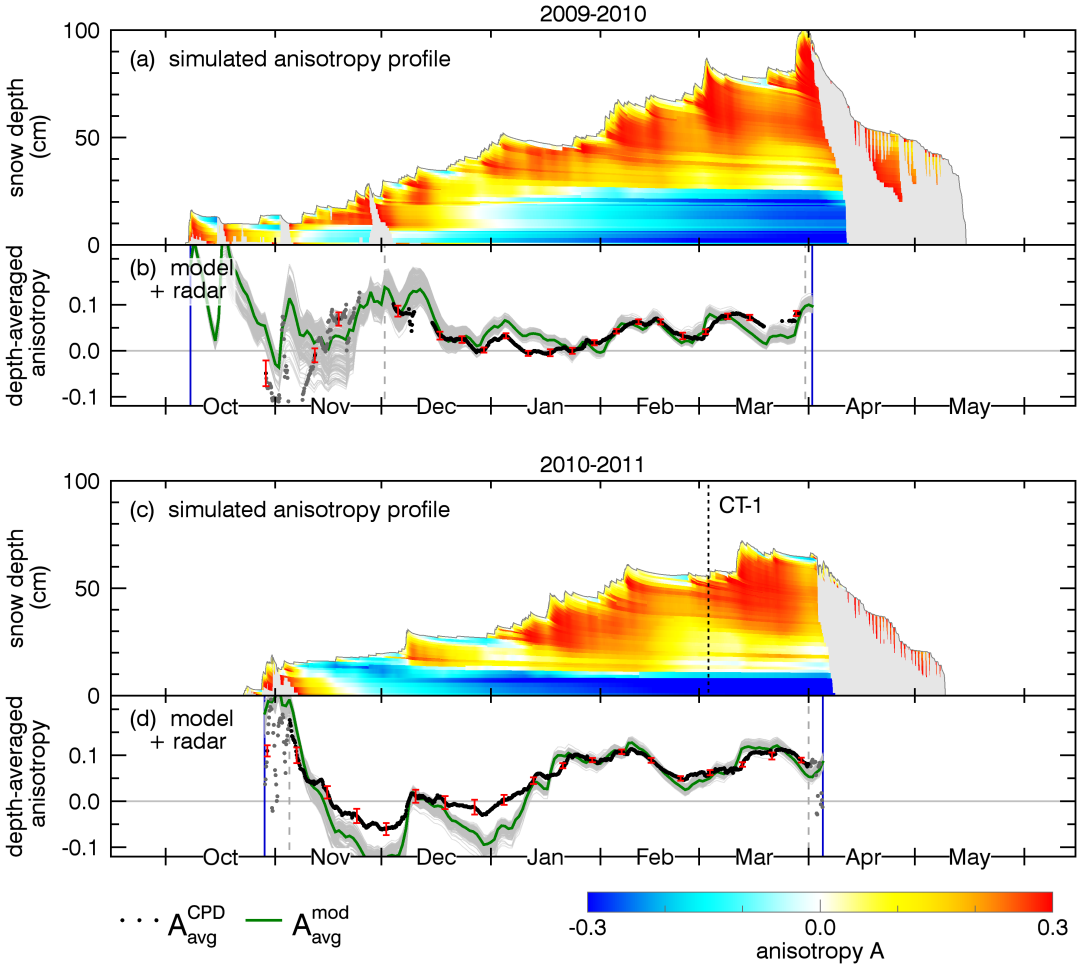

Figure 6. ~~Simulation results~~ Structural anisotropy simulated for the ~~structural anisotropy of the~~ first two seasons 2009/2010 and 2010/2011. (a), (c), ~~in color: time- and~~ depth-resolved ~~modeled~~ anisotropy (in color) based on post-processed SNOWPACK data. Wet snow is grayed out. Model parameters are $\alpha_1 = 0.93, \alpha_2 = 1.68, A_{\min} = -0.7, A_{\max} = 0.3, f_\mu(\cdot) = 1\,\mathrm{mm}$. The dashed line, labeled with CT-1, indicates the sampling date of the CT validation ~~data~~profile. ~~Time-series panels~~ (b), (d): depth-averaged anisotropy of the model $A_{\mathrm{avg}}^{\mathrm{mod}}$ (green~~: ensemble median, gray: ensemble members~~) ~~compared with~~ and radar-measured anisotropy $A_{\mathrm{avg}}^{\mathrm{CPD}}$. ~~Dashed gray lines bound the radar~~ Radar measurements ~~(~~used to calibrate α_2 are shown as black dots~~) used for model calibration~~. Gray dots indicate radar measurements excluded from calibration because of a ~~large~~ too big standard deviation (red error bars).

standard deviation $\sigma(A_{\mathrm{avg}}^{\mathrm{CPD}})$ was below 0.05 . Gray dashed lines limit the radar measurements used for calibration; radar measurements excluded from calibration are shown as ~~the ensemble of gray lines in the background. Begin and~~ gray dots. The begin and the end of the dry snow period are indicated by vertical blue lines. ~~Dashed gray linesbound the period of radar measurements considered reliable enough to determine the free parameters α_1 and α_2 .~~ Short melt events are still visible from the SNOWPACK simulations between the blue lines.

~~It is remarkable that modeled and radar-measured anisotropy ,~~ In the radar measurements the maximum anisotropy never grows much beyond +0.2, even in Dec 2011 where air and soil temperature were around the freezing point such that the growth of vertical structures by TGM was limited and mainly settling of the thick snowpack occurred. We estimate that $A_{\max} \approx 0.3 \pm 0.1$ and used this value in the model.

The depth-resolved, modeled anisotropy is shown in color in the upper panels, (a) and (c) of Figs. 6 and 7. Yellow and red colors indicate horizontal structures and blue colors indicate vertical structures. The model is based on the output of the best snowpack simulation. As we do not model the anisotropy evolution of wet snow, wet snow is grayed out. When the anisotropy profiles are vertically averaged one obtains the simulated, depth-averaged anisotropy, $A_{\mathrm{avg}}^{\mathrm{mod}}$, which is shown as a green line in the lower panels.

To evaluate the uncertainty of the free parameter α_2 we determined it for each season independently and also for all seasons together by minimizing the RMSE between

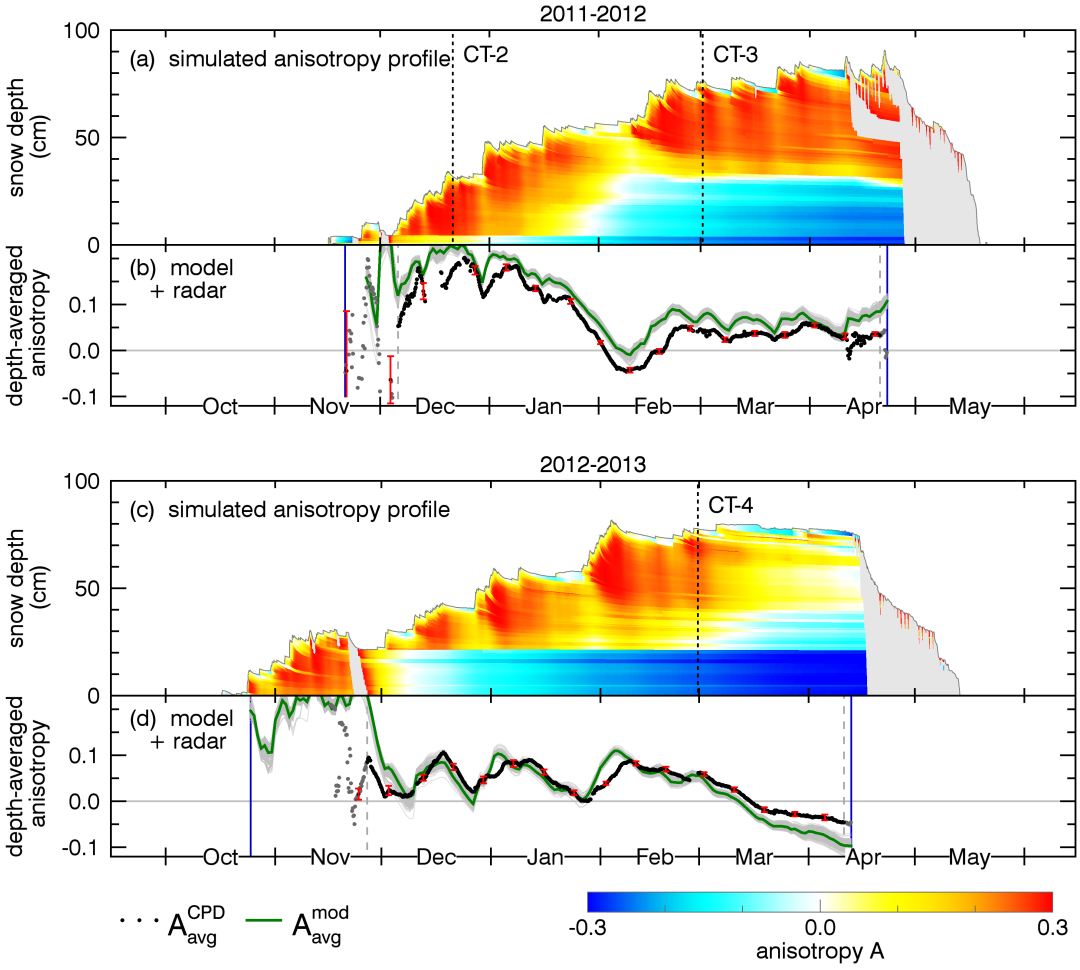

Figure 7. ~~Simulation results~~ Structural anisotropy simulated for the seasons 2011/2012 and 2012/2013. Labels CT-2, CT-3, and CT-4, indicate the sampling dates of the CT validation data. For further details see caption of Fig. 6.

A^{mod}_{avg} and ~~A^{CPD}_{avg}, show ahighly consistent trend: the model is able to catch even small details of the radar measured anisotropy time series. Nevertheless, over some periods, especially in the season 2011/2012, Fig. 7(b), longer systematic deviations persist. For completeness, correlation measures between modeled and measured anisotropy time series are listed in Table 4~~ A^{CPD}_{avg}. Additionally to the RMSE, the model accuracy was measured with the Nash-Sutcliffe model efficiency coefficient and also with the Pearson-r correlation coefficient. Table 4 summarizes the results. The depth resolved profiles and depth-averaged time series in the Figures 6 and 7 show the results for $\alpha_2 = 1.68$ determined for all seasons together which results in an RMSE of 0.033 and a Pearson-r correlation coefficient of 0.89.

The sensitivity of α_2 on slightly different SNOWPACK settings is represented by the ensemble of gray lines in the lower panels of of Figs. 6 and 7. The last column of Table 4 summarizes the ensemble results. The ensemble of gray lines corresponds to $\alpha_2 = 1.87 \pm 0.25$ where the uncertainty is specified by the standard deviation.

Table 4. ~~Correlation between simulated and radar-measured anisotropy, A^{CPD}_{avg} and A^{mod}_{avg},~~ Results for the parameter α_2 determined for each season independently and for all seasons together~~(last row)~~. ~~To quantify the~~ The agreement between model ~~quality~~ and radar anisotropy is given by the ~~following measures are listed: r =~~ Pearson's correlation coefficient (r), ~~NS =~~ the Nash-Sutcliffe model efficiency coefficient (NS), ~~RMS =~~ and the root mean square ~~difference~~error (RMSE). The ~~measures are given for~~ last row contains the ~~best SNOWPACK simulation (left)~~ mean and ~~for the ensemble median~~ standard deviation of α_2 from the ~~best 300 simulations (right)~~ensemble runs.

season	~~r~~ α_2	~~NS RMS~~ r	NS	~~RMS~~RMSE
2009/2010	~~0.88~~ 1.41	~~0.69~~ 0.61	~~0.016~~ 0.25	~~0.85~~ 0.024
2010/2011	2.23	0.97	~~0.85~~ 0.70	~~0.021~~ 0.029
2011/2012	~~0.96~~ 1.02	~~0.67 0.036~~ 0.96	~~0.70~~ 0.92	~~0.035~~0.018
2012/2013	~~0.75~~ 2.08	~~0.30~~ 0.88	~~0.033~~ 0.39	~~0.81~~ 0.031
2009–2013	~~0.84~~ 1.68	~~0.69~~ 0.89	~~0.027~~ 0.55	~~0.86~~ 0.033

Considering, that it is a hypothesis that settling increases the anisotropy, it is remarkable that the modeled anisotropy and the radar-measured anisotropy show a highly consistent trend: the model is able to catch many details of the radar measured anisotropy time series. Nevertheless, in some early winter periods, especially in the season 2010/2011, stronger deviations occur likely because of melt events and differently modeled snow height and layer thicknesses.

From the simulated anisotropy profiles it is evident that snow layers at the bottom of the ~~snow pack always shows a~~ snowpack always show vertical structures (blue, $A < 0$) while the upper snow layers which are stronger affected by snow settling show generally horizontal structures (yellow and red, $A > 0$). ~~However,~~ An exception is the snow surface which shows a more isotropic (and sometimes an even vertical) structure compared to the underlying upper snow layers which experienced more overburden pressure. The occasionally appearing vertical structures at the snow surface are expected ~~because of~~ from the strong temperature gradients at the surface, especially during clear-sky winter nights. During such conditions, TGM transforms the top layers faster than intermediate layers.

A small but very interesting detail~~of both, the model and the radar measurements~~, especially in the radar measurements, is that the anisotropy does not grow instantaneously with accumulating ~~fresh~~ new snow but shows ~~a short delay of a few days . This is clearly visible in both, the anisotropy profiles and the depth-averaged data, after intense snow fall events,~~ an delayed increase within a few days (e.g. in ~~March~~ Mar 2010, ~~March~~ Mar 2011, ~~and February 2013. The~~ Dec 2011, and Feb 2013). We think, the delay results from the fact that it is the settling of ~~fresh~~ new snow which dominantly ~~increases the anisotropy while fresh snow itself~~ and not the anisotropy of new snow itself which does not or only weakly increases the anisotropy. The delay ~~in radar measurements~~ seems to be ~~even more pronounced that the simulated results. Such a delay of~~ more pronounced in the radar measurements than in the model where the anisotropy often increases to quickly after snowfall. The length of this delay was determined to about 2–4 days in average ~~was also observed~~ in (Leinss et al., 2016, Sect. 5.4). ~~Compared to the fast evolution of fresh snow, the model predicts a much slower evolution for old snow with pronounced vertical structures.~~

4.2 Validation with ~~computer tomography~~CT-profiles from the field

The ~~vertically resolved anisotropy~~ seasonally modeled depth-resolved anisotropy was validated with vertically resolved field-measured anisotropy CT profiles. The dates when the CT profiles ~~from computer tomography make it possible to use the CT data for validation. Figure 8 shows simulated anisotropy profiles as blue lines and the CT-based anisotropy as gray dots with a black line indicating the~~

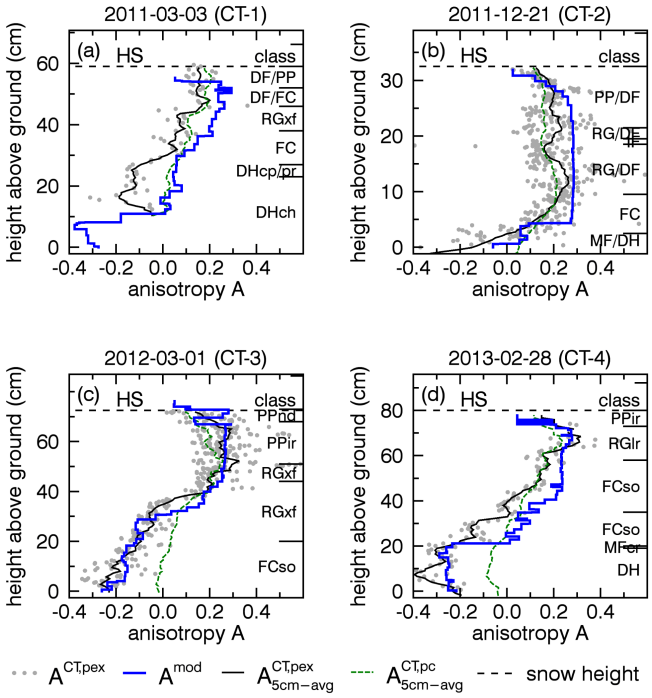

Figure 8. ~~Vertical profiles~~ Comparison of ~~the field-measured~~ simulated anisotropy (A^{mod}, ~~$A^{\mathrm{CT},p_{\mathrm{ex}}}$~~ blue line), ~~determined by computer tomography from exponential correlation lengths~~ with field-measured CT anisotropy profiles ($A^{\mathrm{CT},p_{\mathrm{ex}}}$, gray dots; black line: 5 cm running mean). ~~Green line~~Right axis: snow layer classification according to (Fierz et al., 2009) and measured snow height (HS, horizontal black dashed line). The anisotropy ~~calculated~~ determined from the correlation length p_{c} is shown as a green line (5 cm running mean). ~~Blue line: simulated anisotropy, A^{mod}. Horizontal black dashed line: field-measured snow height (HS).~~ The ~~right axis shows layer classification according to (Fierz et al., 2009) . The four ticks at~~ locations where the ~~top are the mean anisotropy values of~~ CT ~~(p_{ex}), CT(p_{c}), radar (CPD), and modeled anisotropy (mod)~~profiles were taken are shown in Fig. 3.

~~running mean of the CT-based anisotropy. The CT-based anisotropy is derived from exponential correlation lengths p_{ex} according to Eq. 14.~~ were obtained in the field are indicated by vertical black dashed lines labeled with CT-1, -2, -3, and -4 in Figs. 6 and 7.

~~Additional to the anisotropy based on p_{ex}, the anisotropy could also be calculated from other correlation lengths. Being aware, that p_{ex} better characterized length scales relevant for microwave properties, we still compare our results to the anisotropy derived from p_{c}. The length p_{c} is defined by the slope at the origin of the correlation function and describes characteristics on the smallest length scales, e. g. the specific surface area (Löwe et al., 2011). The green dashed line in~~ In Fig. 8 ~~shows the~~ the modeled anisotropy profiles (blue lines) are compared to the CT-based anisotropy (gray dots; black line indicating the 5 cm ~~running mean of the p_{c}-based anisotropy .~~

Table 5. (a) correlation coefficients between ~~the~~ modeled anisotropy profiles ~~calculated from p_{ex}~~ and CT anisotropy profiles as ~~presented~~ shown in Fig. 8. The first three columns are the correlation with respect to the individual anisotropy data points; the rightmost three columns are correlations with respect to the 5 cm running mean of ~~CT-samples. Table (b) shows~~ the ~~depth-averaged anisotropy values from~~ CT ~~, model and radar data~~anisotropy.

(a)	correlation coefficients relative to CT data, p_{ex}					
	CT single samples			CT: 5 cm running mean		
profile	r	NS	~~RMS~~ RMSE	r	NS	~~RMS~~ RMSE
CT-1	~~0.70~~ 0.79	-0.18	0.15	~~0.125~~ 0.84	~~0.79~~ 0.32	~~0.12~~ 0.11 ~~0.14~~
CT-2	~~0.37~~ 0.50	0.10	~~0.148~~ 0.15	~~0.54~~ 0.85	~~0.20~~ 0.40	~~0.147~~ 0.12
CT-3	0.86	~~0.67~~ 0.74	~~0.116~~ 0.10	~~0.95~~ 0.96	~~0.78~~ 0.91	~~0.091~~ 0.06
CT-4	~~0.89~~ 0.91	~~0.61~~ 0.69	~~0.141~~ 0.12	~~0.90~~ 0.92	~~0.67~~ 0.75	

~~Naturally the anisotropy derived from p_c deviates from the anisotropy derived from p_{ex} . This is plausible because a single correlation length cannot represent the complete snow microstructure. Especially for depth hoar, where the anisotropy derived from p_{ex} and p_c differ most, the often used relation $p_{ex} \approx 0.75 p_c$ is not valid any more (Mätzler, 2002; Krol and Löwe, 2016). Indeed, we obtained for depth hoar layers a relation of $p_{ex} \approx 0.8...1.2 p_c$ (Fig.) . Because p_{ex} better describes microwave relevant length scales we focus in the following on comparisons with the p_{ex} -based anisotropy .~~

~~The comparison of simulated anisotropy profiles and CT-profiles shows that the model reproduces the CT-measured profiles in quite a detail (Fig. 8~~running mean). Table 5(a) lists correlation coefficients between the ~~simulated~~ modeled anisotropy and the ~~running mean of the~~ individual CT anisotropy data points derived from p_{ex} ~~-based anisotropy~~ (left columns) as well as ~~correlation coefficients between simulated profiles and the individual CT anisotropy data points derived from~~ the correlation coefficients with the 5 cm running mean of the p_{ex}-based anisotropy (right columns). For ~~the running mean~~both, the Pearson-r correlation coefficients are around 0.8 and higher except for CT-2 (~~$r = 0.54$~~ $r = 0.51$) for which the snow structure does not show much vertical variability except for a thin layer of depth hoar at the bottom of the ~~snow pack.~~ snowpack. Unfortunately for CT-1, Fig. 8(a), no snow samples were taken for the lowest 10 cm.

~~Despite of the good agreement of modeled and measured anisotropy data, a possible deficit of either the model, the definition of the anisotropy , or the determination of the anisotropy by CT can be recognized for negative anisotropies $A < -0.1$~~

4.2.1 Anisotropy determined from p_c

In general, the anisotropy could also be calculated from other correlation lengths. For example, ~~for CT-1 in Fig. 8(a) at a height of the model does not capture several layers that have undergone strong metamorphism. As shown on the right axis, these layers have manually been classified as depth hoar, DHcp/DHch, code according to Fierz et al. (2009). The CT data show clearly vertical structures with $A^{CT} \approx -0.15$. For these layers, depth hoar is also visible in a NIR image, Fig. 9(b), and also in the SNOWPACK grain classification, supplementary~~ the anisotropy A^{CT,p_c} , shown as a green dashed line in Fig. ~~. Unfortunately, no CT-data is available for the lowest because the brittle structure of depth hoar could not be sampled.~~

~~Similar to the discrepancy in CT-1, the model does not reproduce the thick layer of depth-hoar below a melt-crust at the bottom of the snow pack in CT-2 (Fig. 8(b); also visible in the NIR image, 8,~~ is derived from p_c which is defined by the slope at the origin of the correlation function. By definition, p_c describes characteristics on the smallest length scales, e.g. the specific surface area (Löwe et al., 2011) and is not sensitive to the extent of large structures. Therefore, A^{CT,p_c} indicates a less distinct anisotropy than $A^{CT,p_{ex}}$. Especially for depth hoar, where both anisotropies differ most, the often used relation $p_{ex} \approx 0.75 p_c$ is not valid (Mätzler, 2002; Krol and Löwe, 2016) and we obtained rather a relation of $p_{ex} \approx 0.8...1.2 p_c$ (Fig. ~~9(e)). The same holds for the lowest of CT-3 and -4, Figs. 8(c), (d) and the NIR images Figs. 9(d), (e). The lowest of the snow pack in Fig. 8(c) have manually not yet been classified as depth hoar but still as faceted (rounded) grains (FCso, RGxf). Nevertheless, SNOWPACK classified these grains as depth hoar~~ S1).

~~For comparison of the depth-averaged radar data with the CT data, small ticks in Fig. 8, above the snow height line (HS), indicate various depth-averaged anisotropy values: the gray, green, blue, and red ticks are the values of the CT-measured (p_{ex} ,~~ The comparison of the anisotropy profiles based on p_{ex} and p_c ~~), simulated, and radar-measured anisotropy. The radar-measured anisotropy (red ticks) contains a small error range which corresponds to the standard deviation of the radar measurements. Numerical values are provided in Table 5(b).All values are close to zero ($A^{\cdots}_{avg} \approx 0.05 \pm 0.06$), except for CT-2 ($A^{\cdots}_{avg} \approx 0.18 \pm 0.02$) which was sampled after intense snowfall and relatively moderate temperatures such that the effect of TGM was weaker compared to snow setting which resulted in a preferentially horizontal microstructure over the entire depth of the snow pack.~~ shows that p_{ex} is more sensitive to characterize the anisotropy.

4.3 ~~Distribution of fit parameters α_1 and α_2~~

~~The four winter seasons were characterized by quite different snow conditions which made it interesting to determine the free model parameters α_1 and α_2 independently for each season. Furthermore, to analyze their sensitivity with respect to slightly different snow conditions we determined the parameters for each ensemble member of the 300 best~~

~~SNOWPACK simulations. Figure ?? shows a scatter plot of α_1 and α_2 plotted over the global (4-seasons) cost function (Appendix A4) which is indicated by contour lines. Gray dots represent the global solutions α_1, α_2 derived from the entire set of four seasons between 2009 and 2013. Colored dots show the solutions for each of the four winter seasons. Black dots with error bars are the mean and standard deviations of the five different sets of solutions; numerical values are listed in Table ??. All solutions are very close to the global solution except for the 3rd season (2011/2012). This season was characterized by a very fast transformation of of fine grained, horizontally structured snow in Jan/Feb 2012 during very strong average temperature gradients of . The free parameters α_1 and α_2 of this season are about 1.5 to 2-times larger compared to the other seasons.~~

~~Solutions for α_1 and α_2 of all 300 best SNOWPACK runs for different seasons (colors) and all seasons combined (gray). Contour lines show the cost function, Eq. , of all seasons combined. Table ?? lists mean and standard deviation of the set of solutions. Both values are visualized as dots and error bars above.~~

~~Parameter α_1 and α_2 estimated for different seasons. Provided are mean value and standard deviation.season α_1 α_2 2009 / 2010 0.57 ± 0.04 0.44 ± 0.03 2010 / 2011 0.64 ± 0.03 0.35 ± 0.02 2011 / 2012 0.98 ± 0.13 0.72 ± 0.03 2012 / 2013 0.68 ± 0.07 0.41 ± 0.04 2009–2013 0.69 ± 0.04 0.46 ± 0.02~~

5 Discussion

A main motivation of this paper was to show that it is possible to model the radar-measured anisotropy solely based on meteorological data. This was achieved in ~~great~~ detail and demonstrates that polarimetric radar measurements at sufficiently high frequencies (10–20 GHz) can be used to monitor the ~~structural~~ depth-averaged evolution of the ~~snow pack~~ anisotropy nondestructively (Leinss et al., 2016) and even from space (Leinss et al., 2014).

~~Beyond that we provide a model which is able to reproduce the vertically resolved anisotropy that was derived from tomographic reconstruction of the snow pack. Furthermore,~~ Beyond that our results confirm that the creation of vertical structures is mainly controlled by the recrystallization rate of water vapor. The results further indicate a yet undocumented effect of settling on the creation of horizontal structures. We think that it is remarkable that a model, which completely neglects any microstructural parameters like grain size, SSA or snow classification is able to simulate the temporal evolution of a microstructural parameter, the anisotropy, solely based on macroscopic fields ~~. Indeed, the model lacks several details which will be discussed in the following sections after providing a general overview of the model results.~~ and with a very limited set free parameters which we determined from literature values, CT and radar data.

5.1 ~~Discussion of model results and snow conditions~~

~~This section discusses the evolution of the simulated and radar-measured anisotropy with respect to general weather and snow conditions. Snow conditions~~

5.1 Seasonal model results and snow conditions

Snow conditions observed in the field differed significantly between the different winter seasons, therefore we provide a short summary ~~of snow conditions~~ for every season before discussing the evolution of the simulated and radar-measured anisotropy with respect to observed snow and weather conditions. For reference, snow height, air temperature and soil temperature are plotted in ~~Figs. 10 and 10~~Fig. 10.

~~Snow height, air- and soil temperature at different locations (IOA, AWS, MetM = meteorological mast) for the first two seasons, 2009/2010 and 2010/2011.~~

In the first season, 2009/2010, snow fall started early ~~October~~ Oct and accumulated up to 30 cm ~~with~~ during relatively moderate temperatures (and some short melt events) until mid of ~~December 2009~~ Dec when temperatures dropped well below zero and ~~caused soil freezing. Four major snow fall events followed until April when snow melt set it.~~ the soil froze.

The ~~simulated profile for the first season, 2009~~corresponding modeled mean anisotropy varies strongly in Oct/~~2010~~Nov, Fig. 6(~~a), shows astrongly varying anisotropy in Oct/Nov which transforms into vertical structures with the cold temperatures in early January. The following four major~~ b), where model and radar data disagree because microwave penetration was reduced by temporary melt events, gray in Fig. 6(a), and melt metamorphism was anyway not considered in the model. The precision of the radar measurements was also limited by the 10–15 cm thin snowpack. After mid of Nov new snow dominates the modeled anisotropy which agrees then better with the radar measurements. End of Dec cold temperatures transformed the early winter snowpack into vertical structures. Each of the following snow fall events ~~appear as an increase of~~ increased temporarily the average anisotropy~~in~~ , Fig. 6(b). ~~As no CT-data are available for the first season, we provide a~~ The NIR image from 2010-02-23~~in~~ , Fig. ~~9~~9(a)~~. The NIR image~~ , confirms the model results of metamorphic snow (depth hoar) in the lower 30 cm of the ~~snow pack~~ snowpack and shows multiple distinguishable layers above. ~~In Oct/Nov 2009 model and radar measurements do not agree because the thin snow pack results in a very imprecisely radar-measured anisotropy (green line vs. gray dots in Fig.6(b)). Additionally, because of limited microwaves penetration, short surface melt events~~

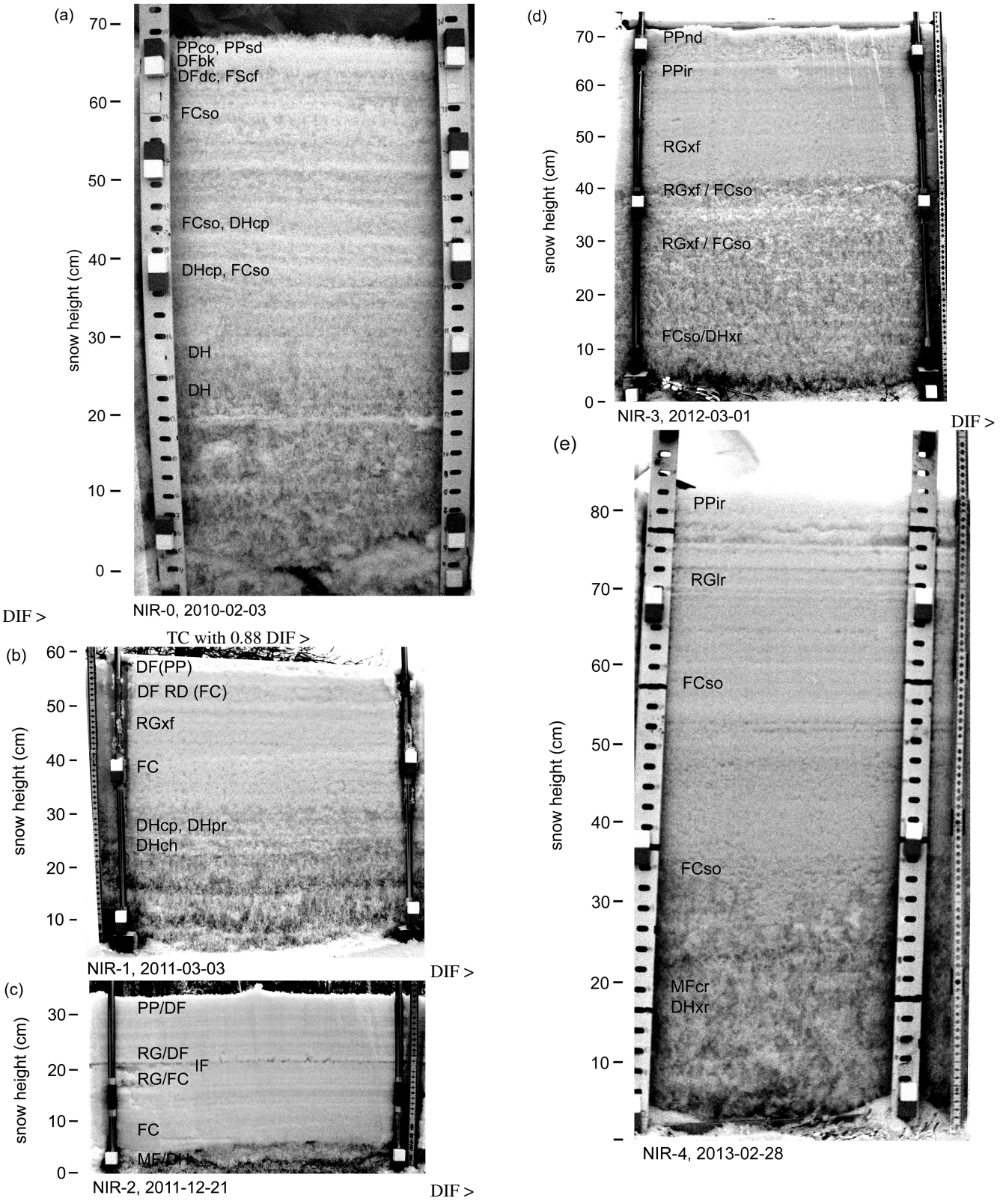

Figure 9. NIR Photography of the ~~snow pack~~snowpack. The image NIR-0 was acquired in the first season on 2010-02-23 where no CT data is available. The other images NIR-1, -2, -3, -4 corresponds to the CT-profiles CT-1, CT-2, CT-3, CT-4. The intensity of the NIR photography is mainly determined by grain size but also shows ~~nicely~~ the metamorphic state of the ~~snow pack~~snowpack. The NIR ~~photographs provide~~ photography provides an independent measure for the absolute depth of individual snow layers and ~~help~~ helps to identify strong structural transition in the ~~snow pack~~snowpack.

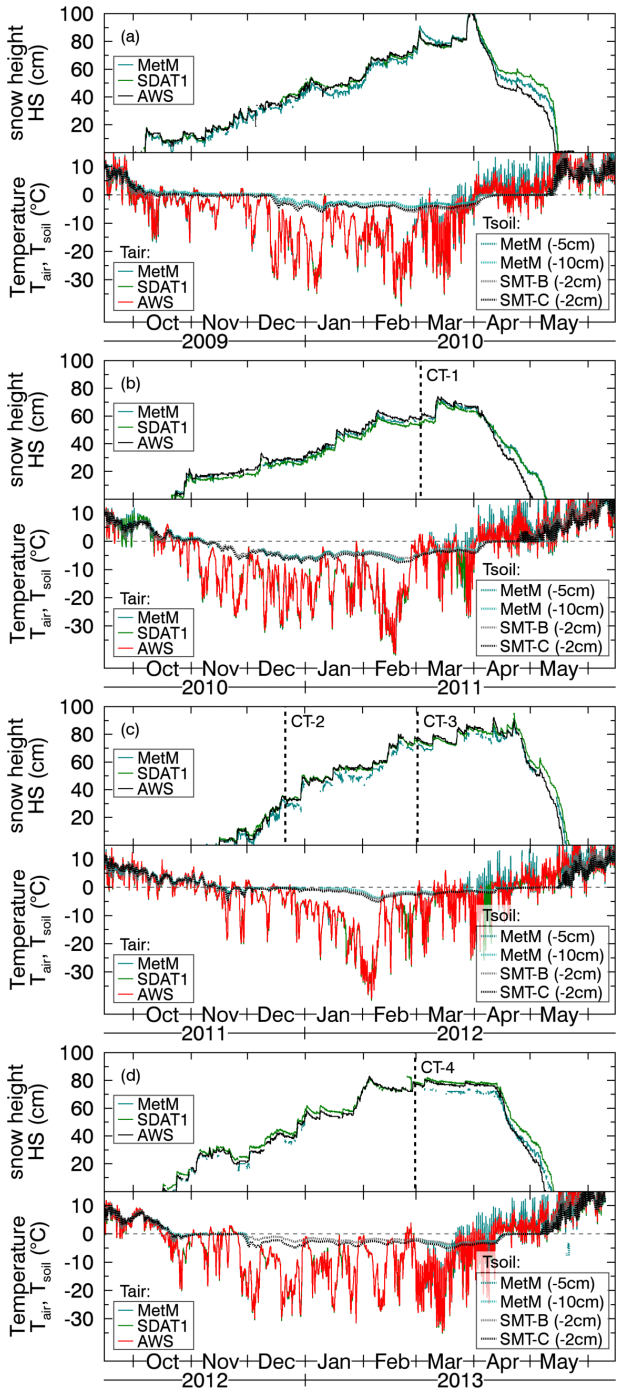

Figure 10. Snow height, air- and soil temperature at different locations (IOA, AWS, MetM = meteorological mast)~~for the last two seasons, 2011/2012 and 2012/2013.~~.

~~appear as radar-anisotropy values around zero.~~ No CT validation data is available for the first season.

In the second season, 2010/2011, conditions are characterized by ~~cold temperatures below already in early November combined with a shallow snow pack such that soil freezing occurred in the second week of November. Until January snow height was less than 30 cm and an over 20 cm thick layer of~~ a shallow snowpack with less than 30 cm snow until Jan, accompanied with cold temperatures. The soil froze already mid of Nov and a layer of 20 cm depth hoar was present during the entire season~~(NIR image~~.

The modeled mean anisotropy, Fig. ~~9(b)).~~

~~The simulated profiles for the second season, 2010/2011, Fig. 6(c), shows that the snow from early November transformed to vertical structures within 2–3 weeks. These vertical structures~~ 6(d), clearly shows vertical structures until Jan but the radar data indicates a less strong anisotropy. During this period, the uncertainty of the radar data, indicated by the standard deviation (≈ 0.03 , red error bars), is higher compared to other periods which could hint at some systematic measurement errors (Sect. 5.3). The modeled, depth-resolved results shows that these vertical structures persisted through the entire winter season. In the ~~radar-signal in~~ NIR image, Fig. ~~6(d), the vertical structures appear clearly as a negative signal until January after which of additional snow accumulated. The comparison with~~ 9(b), these structures appear as a 20 cm thick depth hoar layer at the bottom of the snowpack, which could not be sampled for CT analysis due to its brittle structure. For the upper 50 cm, the model overestimates the CT-measured anisotropy but still agrees with the general trend of the CT data from 2011-03-03, Fig. 8(a)~~, shows a good agreement in the upper snow layers but a significant discrepancy between 10 and where the model predicts positive values $A^{\mathrm{mod}} \approx 0.05$ but the CT data show negative values $A^{\mathrm{CT,p_{ex}}} \approx -0.15$~~ .

In the third season, 2011/2012, snow fall started ~~later as usual, but during December 2011 about~~ late but with intense snow fall 50 cm of snow accumulated in Dec during very mild air temperatures, often above -5°C. ~~As settling dominated TGM, almost the entire snow pack showed a horizontal structure until mid January (~~Except for a few days in early Dec, TGM was almost not present and field measurements report finer grain size compared to other winter seasons (Leppänen et al., 2015). Then, between Jan and early Feb, temperatures dropped gradually from -10°C to -30°C and strong TGM set in which transformed the fined grained snow visible in Fig. ~~7(a) and CT-2~~ 9(c) into the faceted crystals shown in Fig. ~~8(b)). Only a few-centimeter thick~~ 9(d).

The modeled mean anisotropy, and also the radar measurements, show the highest observed values, $A \approx +0.2$, because in Dec vertical structures were almost completely absent. Only a thin layer of depth hoar ~~(below a melt-crust layer) was present which is , similar to the previous season, only poorly represented by the simulation. The mild temperatures in December caused very weak TGM which preserved the fine-grained snow, clearly~~ is visible in the ~~NIR photo~~ modeled results, Fig. ~~9(c). Mid-January to early February, temperatures dropped gradually from -10C to -30C and strong TGM set in (compare Fig. 9~~7(a),

which is confirmed by NIR and CT data, Figs. 9(c) ~~with~~ and 8(b). With the strong TGM in Jan/Feb the initial snowpack transforms quickly into a 30 cm thick layer with vertical structures which emerges as a strong anisotropy reversal in Fig. ~~9(d))~~7(b). Then, mid of ~~February about~~ Feb, additional 30 cm of ~~fresh snow accumulated ontop of the strongly transformed lower layerswhich is visibly by the settling-induced horizontal structures ($A \approx +0.25$) in the upper of the snow pack in the anisotropy~~ new snow fell on top of the transformed layers, resulting in the step-like anisotropy transition in the profile CT-3 ~~,~~ shown in Fig. 8(c). ~~After that~~Until Apr, several minor snow fall events ~~repeated until snow melt end of April which appeared~~ appear as little oscillations in the depth-averaged and radar-measured anisotropy, Fig. 7(b).

~~It is worth to note that for the period Jan/Feb 2012, both the simulation, Fig. 7(a), and the comparison of the CT-profiles (CT-2 and CT-3~~ At the end of the third season, gray snow layers appear in Fig. ~~8) show that the entire snow structure transformed from horizontal to vertical structures. However, the model was not able to track the fast decay of the anisotropy between January and February 2012 and generated too positive anisotropy values for the minimum mid of February ($A^{\mathrm{mod}}_{\mathrm{avg}} \approx 0$, Fig. 7(b)) for which anegative average anisotropy of $A^{\mathrm{CPD}}_{\mathrm{avg}} \approx -0.05$ was measured by radar. Field measurements and CT data show that in the early winter 2011/2012 finer grain sizes were observed compared to other winter seasons (Leppänen et al. (2015) and SSA data in Fig.) . It is likely, that the fine grains transformed faster than represented by the model. The resulting offset of a systematically too positively modeled anisotropy persists from February until snow melt. Except for the offset, the subsequently simulated anisotropy variations agree well with the radar-measured anisotropy.~~

~~At the end of the third season, from~~ 7(a) from 10–13th of ~~April~~ Apr 2012 ~~,~~ after accumulation which indicate that wet snow and rain fell ~~ontop of the snow pack which froze afterwards. This causes an interesting feature at the end of the season in Fig. 7(b): the rain-on-snow event appears as a dip in the previously positive values of the radar-measured anisotropy. This event coincided with strong settling and the influence of the latter on the anisotropy was balanced by adjusting the melt metamorphism term, Eq. . In contrastto the dip in the radar measurements , the simulated time series (green line in Fig. 7(b)) shows a positive peak in the average anisotropy indicating strong snow settling. This apparently opposite trend likely results from limited microwave penetration into the wet snowduring the time when settling of the wet snow was strongeston~~ top of the snowpack which partially refroze afterwards. The event induced strong settling in the SNOWPACK model which in turn increased the modeled anisotropy (green line, $A^{\mathrm{mod}}_{\mathrm{avg}} \approx 0.06$). In contrast, the radar measurements reach for a moment zero (no penetration into wet snow) but returned to the previous values $A^{\mathrm{CPD}}_{\mathrm{dvt}} \approx 0.03$. We think that the anisotropy increase induced by settling was compensated by an anisotropy reduction from melt metamorphism which is currently not included in the model.

In the last season, 2012/2013, conditions are characterized by four major snow fall events~~and almost no precipitation from February until April 2013. During the period of the first snow fall events in November, temperature was frequently at 0C such that~~ . During the first event in Nov occasionally surface melt occurred. After the last event in Feb, very little precipitation was measured and cold temperatures persisted until early April.

The modeled mean anisotropy in Nov is above $+0.2$ but because of frequently surface melt no reliable radar measurements were possible (~~initial "noise"indicated by~~ gray dots in Fig. 7(d)). ~~The last dip~~ Still, for a few days mid of Nov, anisotropy values up to $+0.2$ are visible in the radar ~~data end of November 2012 (gray dots in Fig. 7(d)) is an indicator for increasingly~~ measurements but they quickly approached zero, likely because of decreasing microwave penetration into wet snow. ~~This goes along with positive temperatures (Fig. 10) and also simulated liquid precipitation (Fig.) which caused a height loss of about 10 cm due to rain on snow which was not correctly simulated by SNOWPACK (see also Fig. 17). As a consequence SNOWPACK modeled not enough precipitation mid of December; therefore, the peak in the mean modeled anisotropy (mid of Dec 2012 in Fig. 7(d)) which indicates horizontal structures is too small compared to the radar data. Then, starting from December 2012, the simulated anisotropy, Fig. 7(c), shows a persistent~~ With very cold temperatures around -20°C end of Nov, the snowpack refreezes and the positive anisotropy recovers but then quickly decays due to strong TGM resulting in a 30 cm thick layer of depth hoar which continued to evolve during the remaining season, Fig. 7(c). ~~This depth hoar layer formed after the melt event end of November after which air temperatures suddenly dropped to around -20C.~~ This depth hoar layer reached the lowest anisotropy values observed ~~$A^{\mathrm{CT},p_{\mathrm{ex}}} \approx -0.3 \pm 0.1$ (~~in the field $A^{\mathrm{CT},p_{\mathrm{ex}}} \approx -0.4$ as shown in CT-4 in Fig. 8(d)~~). Similar to the season 2010/2011, the model seems either to overestimate such low anisotropies or the CT-data underestimates the anisotropy of depth hoar layers. Nevertheless, the average anisotropy of the remaining season was well simulated, Fig. 7(d).~~ .

Interesting in ~~March and April~~ Mar and Apr 2013, and also in other seasons, are the modeled vertical structures ~~close to~~ at the snow surface~~which also appeared in other seasons. These are explained by strong snow surface temperature gradients which act on the snow at the surface while this snow~~ . These result from strong temperature gradients modeled in the snow surface which does not experience any overburdened pressure and can therefore quickly transform into vertical structures or possibly surface hoar as classified by SNOWPACK (Figs. S20).

5.2 ~~Discussion~~ Quality of meteorological input data

For best ~~results of the anisotropy model~~ modeled anisotropy results it is critical that both, meteorological input data and snow properties simulated by SNOWPACK are as correct as possible. For most of the meteorological data this was ensured by ~~redundant sensors as shown in Figs. 10 and 10 and discussed in Appendix A1 (for data of all sensors see Fig. –). Only precipitation and solar radiation required some calibration. Precipitation was adjusted using~~ using redundant sensors, only precipitation was adjusted by SWE measurements (~~Appendix A1). Still, some inaccuracies in precipitation data can be detected by comparing measured and modeled snow height, Fig. 16. Radiation data was homogenized and gaps were filled as described Appendix A2. The gaps can be found in~~ details in Appendix A1, for raw data see Figs. S3–S6~~or likewise in Fig. . Solar radiation was calibrated implicitly by calibration of SNOWPACK as described in Appendix A3. Unfortunately, snow temperature measurements, used for calibration, contained also some unrealistic values. In the following we discuss which gaps and errors in radiation, precipitation and snow temperaturecould have affecting the simulated anisotropy~~). The results of SNOWPACK were assessed with snow depth and snow temperature.

For ~~snow temperatures,~~ Feb 2011 we noticed that ~~in February 2011,~~ when air temperatures dropped below -30°C ~~, modeled~~ measured snow temperatures were 10–20 K ~~higher than measured~~ lower than modeled snow temperatures (~~red vs. black~~ black vs. red lines, 2nd column in ~~Figs. 16 and 17~~Fig. S17). We ~~are quite confident~~ think that this is a measurement error because ~~for the~~ temperatures 10 cm above ground should not deviate strongly from measured soil temperatures, especially below a 60 cm ~~thick mid-winter snow pack it is physically unrealistic that the measured snow temperature at above ground deviates strongly from the measured soil temperature 5 cm below ground. A similar effect might have occurred in~~ thick snowpack. Similar for Feb 2010~~where measured snow temperatures~~ , snow temperatures measured 50 cm above ground were ~~about 10 K colder~~ 10 K lower than modeled temperatures. The reason could be a few cm deep snow pit at the sensor array as mentioned in Sect. 3.3.1. Fortunately, for both events, ~~the~~ modeled temperature at the bottom of the ~~snow pack agrees very closely to the measured soil temperature~~ snowpack agree closely with measured soil temperatures (red vs. gray line~~in the~~ , second-last row ~~of Figs. 16 and 17~~in Fig. S17). Hence, we are confident that SNOWPACK ~~generally~~ simulated quite reasonable snow temperatures.

~~For the long wave radiation data in the~~ Snow temperature, especially in the upper layers, is strongly affected by the radiation balance which in turn affects settling, snow melt and TGM. Therefore, wrongly interpolated gaps in the radiation data cause deviations in the modeled anisotropy. For example, in the first season, several ~~multiple day long gaps~~ gaps of multiple days in the long wave radiation data between Dec 2009 and Jan 2010 were interpolated~~and the results seems to be fine: modeled and measured snow height agree within a few cm when snow height was not enforced (Fig. 16) and SWE agreed within when snow height was enforced (Fig. 17). Nevertheless,~~ Likely, too high incoming long wave radiation in the first week of ~~January~~ Jan 2010, resulting in modeling of a too warm snow surface, could explain why the anisotropy in ~~January~~ Jan 2010 did not decrease as indicated by the radar measurements, Fig. 6(b).

In the second season, several gaps of multiple days in the long wave radiation data between Nov 2010 and Jan 2011 seem to be correctly interpolated as both, snow height and SWE agree very well; ~~for this period, simulated snow temperatures look reasonable. Also,~~ nevertheless, the simulated anisotropy ~~looks reasonable and agrees well with~~ deviates from the radar data. In the third seasons, radiation data was complete ~~and missing radiation data in Oct 2011 can be ignored because of snow free conditions.~~

during winter. In the forth season, the radiation balance for the rain on snow event ~~, mentioned in the previous section for~~ in late Nov 2012 ~~, was not correctly modeled by SNOWPACK. Although snow height was enforced, apparently no snow height loss was simulated (Fig. 17). This, possibly because of a gap in the radiation data where the actual incoming long wave radiation was likely higher than interpolated for the simulation. Simulated snow temperatures well below zero (Nov 2012, last column of Fig. 17) support the hypothesis that incoming long wave radiation was filled with too low values. Because snow height was enforced, the too large snow height end of Nov implied forcing with too low precipitation for mid of Dec which resulted in less fresh snow with a positive anisotropy and in turn explains why the simulated anisotropy is lower than the radar-measured anisotropy, Fig. 7(d).~~ was manually corrected (Appendix A2).

Missing short-wave reflection data were no problem, because short wave reflection was estimated based on the the simulated albedo. The incoming short wave radiation data did not contain any significant gaps.

5.3 ~~Model deficits~~Precision of radar measurements

~~In the model, we neglected any microstructure and instead introduced free parameters which were determined by the radar data. As single parameters cannot represent the underlying dynamics of the microstructure we discuss here the free parameters and neglected microstructural effects.~~

~~The scatter of the free modelparameters α_1 and~~ Deviations between model and radar data could result from measurement errors and assumptions in the electromagnetic model to derive the anisotropy from the CPD. Uncertainties in the radar data could affect the strain-parameter α_2 and $A_{\max}$. Of these, only α_2 ~~provides an uncertainty range and characterizes how specific these parameters are for each~~

~~season. In general, their values are close together, except for the set of parameters which provides the best solution for~~ was solely determined by radar whereas the value for A_{max} is also constrained by CT data.

The uncertainty of $\alpha_2 = 1.0..2.5$ results very likely from model deficits rather than from radar measurements. The anisotropy measured with radar at different frequencies and incidence angles agrees within the standard deviation (shown in Figs. 6 and 7) with the underlying model (Leinss et al., 2016, Sect. 5.2). Systematic errors could result from uncertainties of snow density estimations $\rho_{\mathrm{snow}} \approx 0.2 \pm 0.05$ which would result in an anisotropy error of less than 10% (Leinss et al., 2016, Fig. 3).

5.4 Anisotropy model deficits

It may surprise that we neglected any parametrization of the microstructure in the model. For example, instead of fixing $f_\mu(\cdot) = 1\,\mathrm{mm}$, a more physical approach would be to characterize each grain type and size by its potential velocity to transform into vertical structures by implementing a more sophisticated definition of $f_\mu(\cdot)$. However, with the first approximation by setting f_μ equal to grain size, $f_\mu = r_{\mathrm{g}}$, to weight the TGM-term by the inverse of the ~~third season (blue dots in~~ grain size to allow for faster transformation of smaller ice grains, we could not produce reasonable results. Instead the strong dependence on grain size caused a strong vertical variability of the anisotropy combined with a too slowly changing anisotropy for depth hoar with very large crystals (Fig. ~~??). For this season,~~ S27).

Similar to SNOWPACK, we did not consider any coupling of TGM and the settling rate as observed by Wiese and Schneebeli (2017). Instead we fitted the free parameter α_2 to radar data and determined the ~~values are almost twice as large as for the other seasons. Fig. ?? provides anisotropy profiles of all four seasons but which were calculated for $\alpha_1 = 0.98$ and $\alpha_2 = 0.72$ as determined for the third season . For this realization of the model, the mean-anisotropy shows stronger short-term variations, similar to overshooting, compared to the anisotropy measured by radar.Nevertheless, for this configuration the simulation results seem to agree better with the CT-data, especially for strongly metamorphic snow.We conclude from that~~ uncertainty $\alpha_2 \approx 1.0..2.5$ by independent fits for each season and for different SNOWPACK ensemble members (Table 4). Interestingly, and likely because of the bounds A_{min} and A_{max}, model results do not differ significantly within the uncertainty range of α_2 (compare Figs. 6 and 7 with Fig. A3). Therefore we conclude that the mean value $\alpha_2 \approx 1.7$ is a good approximation which can be used for any snowpack.

Note however, that the ~~range of α-values provided in Table ?? reflects a similar uncertainty as the uncertainty for the anisotropy profiles calculated from CT data (see next section)~~analysis is presently limited to the prediction of anisotropy from the output of a snowpack model (no feedback). If the (existing) feedback of the anisotropy onto mechanical properties of snow was allowed for, the parameters in the strain term will certainly change. We also need to point out that currently no comprehensive laboratory data exists which confirms the modeled relation between settling of fresh snow and the creation of horizontal structures.

~~It is remarkable how well the model reproduces the radar-measured anisotropy time series. Nevertheless, it may surprise that the model completely neglects any dependence on grain size. However, we found that no simple grain size dependence, like weighting the TGM-term by the inverse grain size (by setting the microstructural parameter equal to grain size, $f_\mu = r_{\mathrm{g}}$ in~~ In the model we also neglected any melt metamorphism which could transform the microstructure very fast. We think that for our Finnish data, melt metamorphism can be neglected as no strong melt events occurred except during the spring snow melt where no radar data is available. Therefore, calibration of a melt-metamorphism equation would lack sufficient calibration data. Nevertheless, we like to suggested here a simple model. We think that the surface tension of water should cause a rounding of ice grains which would drive any anisotropic structure towards isotropy. Unfortunately, observational data and models to predict melt metamorphism are still rudimentary and except for the model and references in (Lehning et al., 2002a) and (Brun et al., 1992) we could not find any detailed studies. Similar to their given rate equations we tried to model the anisotropy decay due to melt metamorphism as

$$\dot{A}_{\mathrm{melt}} = -\alpha_3 A \cdot \theta_{\mathrm{w}}^{\mathrm{v}\,3} \tag{15}$$

with the empirical constant $\alpha_3 \approx 2 \cdot 10^{-3}\,\mathrm{day}^{-1}$ and the liquid water volume fraction $\theta_{\mathrm{w}}^{\mathrm{v}}$ in vol.%. The parameter α_3 was determined from only one event in Apr 2012 where the snow refroze after strong surface melt occurred. Despite of strong settling during the spring snow melt, Eq. ~~5), could produce reasonable simulation results~~ (15) lead to almost isotropic conditions after one week (Fig. S26). ~~Using the relation $f_\mu = r_{\mathrm{g}}$ caused a strong vertical variability of the anisotropy combined with too positive values for the anisotropy of depth hoar (Fig.). We still think that neglecting the microstructure could be the main reason why the model was not able to simulate the fast decay of horizontal structures in Jan–Feb 2012.~~

The initial anisotropy A_{ini} was assumed to be constant and close to zero. Model results support this assumption and provide reasonable results for A_{ini} between 0.00 and 0.05. The profiles CT-2 and CT-3, Fig. 8(b) and (c), also show a slightly positive anisotropy, 0.05 ± 0.05, for the surface layer 2–3 days after snowfall and support the assumption that the initial anisotropy must be small. Within the given range for A_{ini}, a weak temperature dependence for A_{ini} might

exist, but no representative data is available. We think that stronger cohesion between crystals near the melting point could lead to a more isotropic structure (but with faster settling) compared to cold temperatures where crystals align rather by gravity and their anisotropic shape. A temperature dependence for the shape of snow growing in the atmosphere (Libbrecht, 2005) could also influence the initial anisotropy and the subsequent evolution of the anisotropy. This, because different grain types (dendrits vs. graupel would be extremes) should show a different settling behavior and likely also a differently strong anisotropy evolution under TGM.

Beyond the ~~dimensions~~ spatial distribution of the microstructure which determines the structural anisotropy (the grain shape), we ignored the crystallographic fabric of snow, i.e. the angular distribution of the orientation of the c-axis of the hexagonal ice crystals ~~which compose the microstructure~~(the crystal lattice orientation) which affects not only the dielectric anisotropy but also the crystal growth dynamics. For the radar data it was ignored because the snow fabric anisotropy affects only very weakly the dielectric anisotropy~~(Appendix A in Leinss et al. (2016))~~: $\Delta A \ll 0.02$, (Leinss et al., 2016, Appendix A). For the model, we neither consider the evolution of the snow fabric anisotropy nor the influence of ~~crystal orientation~~ snow fabric (crystal orientation) on the evolution on the structural anisotropy. This, because only very few studies exist which provide experimental insight about the orientation of the snow fabric (Calonne et al., 2016) or even the temporal evolution of the snow fabric anisotropy (Riche et al., 2013). Furthermore, the dominant growth direction of snow crystals depends on temperature (Lamb and Hobbs, 1971; Lamb and Scott, 1972) and is not necessarily parallel to the temperature gradient (Miller and Adams, 2009) as it can be clearly observed in ~~the supplementary movie in (Pinzer et al., 2012). Motivated by the~~ (Pinzer et al., 2012, supplementary movie) . The competing effect of ~~crystal orientation, structural disorder and structural~~ growth direction by crystal orientation versus structural optimization to increase entropy production by increasing the vertical thermal conductivity ~~(Staron et al., 2014) we simply introduced a lower limit~~ as suggested by Staron et al. (2014) might be a reason why a lower limit $A_{\min}$ of the anisotropy ~~$A_{\min}$ under TGM~~ during TGM exists and why no perfectly vertically oriented snow structure has been documented.

5.5 ~~Characterization~~ An undocumented effect of ~~the microstructure~~settling?

~~As observed in Sect. 4.2 and discussed in Sect. 5.1,~~ From the radar time series a clear increase of the anisotropy a few days after snow fall is revealed in (Leinss et al., 2016, Sect. 5.4) and also in (Chang et al., 1996, Fig. 7). Likewise, space borne data indicates an increase of the CPD (and hence the dielectric anisotropy) proportional to the amount of new snow which must have settled after deposition (Leinss et al., 2014, Fig. 12). In our model this settling-induced creation of horizontal structures is well predicted by describing the anisotropy changes proportional to the strain rate. The modeled effect is however not independently confirmed yet and existing studies about the anisotropy evolution under strain provide very limited insight to confirm our hypothesis.

For example, Wiese and Schneebeli (2017) did not observe any significant growth of horizontal structures during compaction of, however, relatively dense and coarse snow ($\rho_{\text{snow}} \approx 250\,\text{kg}\,\text{m}^{-3}$, SSA = $13\,\text{m}^2\ \text{kg}^{-1}$) which has also sintered for several months after initial sample preparation by sieving. Still, most samples showed a slight horizontal structure at the begin of the experiment. Different to Wiese and Schneebeli (2017) and with the aim to study new snow of relatively low density ($\rho_{\text{snow}} \approx 100\,\text{kg}\,\text{m}^{-3}$ and SSA = $70\,\text{mm}^{-1}$ = $76\,\text{m}^2\ \text{kg}^{-1}$) Schleef and Löwe (2013) avoided any sintering and observed indications for "the anisotropic nature of densification" by attributing observed density changes "solely to a squeeze of the structure in the vertical direction, i.e. to axial strains". The affine compression in our model reflects this squeeze.

From our modeled results and from the above described experiments and findings, we conclude that a so far undocumented effect during settling exists which creates horizontal structures, at least during an initial phase after new snow deposition. Unfortunately, a reanalysis of the dataset from (Schleef and Löwe, 2013; Schleef et al., 2014) comprising 700 CT images is clearly beyond the scope of the present study, also because the present calculation of the ~~largest deviations between the modeled and CT-measured anisotropy were found for depth hoar, where the modeled anisotropyis less negative than suggested by the CT-measurements based on p_{ex} . Interestingly, the model agrees well with anisotropy derived from p_{c} . However, we believe that the better agreement between the model and~~ anisotropy from CT images may break down in new snow (next section).

5.6 Anisotropy calculations from CT

Deviations between model and CT data could also result from uncertainties in the definition of the anisotropy from ~~p_{c} compared to p_{ex} is a coincidence which is not of further benefit for~~ the ~~interpretation of the radar measurements. This is supported by Fig. ?? where the parameters α_1 and α_2 determined for the third seasons 2011/2012 have been applied to all four winter seasons and where the simulated anisotropy is closer to the anisotropy derived from p_{ex} .~~

~~The origin of this discrepancy for depth hoar is not clear, especially in the context that for the second season the radar time series and the simulation, Fig. 6(d), agree best compared to other seasons (Pearson-$r > 0.97$, Table 4) while for this season the correlation with CT-data is the lowest (Table 5). We think that a combination of the following factors might~~

~~have lead to the observed discrepancy: 1) uncertainties of the model to describe the dynamics~~ microstructure. To understand this we recall that the anisotropy of the ~~anisotropy for depth hoar, 2)uncertainties in~~ dielectric tensor is characterized by a second rank fabric tensor that is defined by an integral over the anisotropic correlation function of the ~~CT-measurements where, especially for large depth hoar crystals, sample size effects could lead to biased estimates of correlation lengths, here of~~ material (Rechtsman and Torquato, 2008). Under the assumption that the correlation function possesses ellipsoidal symmetry, i.e. has the form $C(r/\ell(\cos\theta))$ with a single size scaling function $\ell(\cos\theta)$ that depends only on the polar angle θ , this integral can be evaluated exactly. The resulting fabric tensor can then be expressed in terms of the ratios of correlation lengths. If ellipsiodal symmetry was strictly true, any derived length scale (p_{ex}, ~~3) uncertainties how well the anisotropy derived from the microwave permittivity can actually be compared to the anisotropy determined from p_{ex} , and 4) uncertainties from depth-averaging of the model data and the assumption of a homogeneous (depth-averaged) density for the radar-determined anisotropy.~~

~~Because the model was written to explain the microwave measurements it could be biased towards the anisotropy derived from radar.On one hand the assumption of an exponential correlation functions seems to be more applicable to depth hoar than other snow types (Krol and Löwe, 2016) but on the other hand, we expect in general higher uncertainties of estimated p_{ex} for large structures (depth hoar) because of larger statistical fluctuations of the correlation function in finite samples. A systematic analysis of the representative elementary volume for the two point correlation function is however presently missing. Therefore it remains elusive which of the mentioned factors is the most important one.Further studies on sample size effects and combined radar and CT measurements could elucidate this problem.~~

$p_{\mathrm{c}}, \ldots$) could be used for the anisotropy calculation and should lead to the same result. This is however not the case, as shown in Fig. 8 where we compared the anisotropy based on the two correlation lengths p_{ex} and p_{c} . On physical grounds, it is ~~also reasonable to expect~~ reasonable that p_{ex} rather than p_{c} is better suited to characterize the structural anisotropy ~~in the dielectric tensor because~~ for microwave measurements: p_{ex} characterizes the snow structure on length scales which are (still small but) closer to the wavelength of the radar. In contrast, density fluctuations on the smallest scales (namely those characterized by p_{c}) solely characterize local properties of the ice-air ~~interfaces and the anisotropy calculated in (Löwe et al., 2011) from p_{c} seems to be irrelevant for the~~ interface (Löwe et al., 2011) which are irrelevant features for radar wavelengths. ~~To understand this we recall that the anisotropy of the dielectric tensor is characterized by a second rank tensor that is computed by an integral over the anisotropic correlation function of the material (Rechtsman and Torquato, 2008). Under the assumption that the correlation function has an ellipsoidal symmetry, this integral can be evaluated exactly to express the anisotropy via ratios of exponential correlation lengths in different directions when computing the parameter Q that determines the eigenvalues of the structural fabric tensor. This has been done in (Leinss et al., 2016, Appendix C) for the dielectric permittivity and in (Löwe et al., 2013) for the thermal conductivity leading to an very good agreement with simulations. It must be noted though, that the validity of the assumption of an ellipsoidal symmetry of the correlation function was never investigated in detail. In addition, the mere characterization of snow solely by three (exponential)~~ The experiments from (Löwe et al., 2011) provide yet another hint for the violation of a (strict) ellipsoidal symmetry: It was shown the two-point correlation function contains at least two characteristic length scales which exhibit different ratios in different coordinate directions, again incompatible with the ellipsoidal form. In summary, there are indications that the current (approximative) calcluation of the anisotropy from a CT image using exponential correlation lengths is ~~also an approximation (Krol and Löwe, 2016) which renders an estimation of (likely existing) uncertainties of CT-based p_{ex} estimates rather difficult. Here simulations of computer-generated two-phase media with prescribed correlation and anisotropy structure might be a remedy (Tan et al., 2016)~~not equally well justified for different snow types. This may also explain observed differences between modeled and CT-based anisotropy and definitely needs to be taken into account in a potential assessment of strain effects on the anisotropy evolution in snow.

6 Conclusions

In this paper, a model for the temporal evolution of the structural anisotropy of snow was designed. The model is based on simple rate equations and requires solely the ~~folowwing macroscopic fields~~ following macroscopic fields as input variables: strain rate, temperature and temperature gradient~~of the snow pack~~, ideally depth-resolved~~, as input variables~~. These variables are provided by most of the more advanced ~~snow pack~~ snowpack models, here we used SNOWPACK. ~~In the model, the~~

To describe the evolution of the anisotropy~~is driven by the following three contributions: snow settling leads to a preferentially horizontal structure,~~ , the model considers only two contributions: temperature gradient metamorphism ~~causes growth of~~ (TGM) which was confirmed to create vertical structures and ~~melt metamorphism causes rounding of the structures. The three contributions are balanced by free parameters which were calibrated by minimizing the difference between the modeled anisotropy and anisotropy~~ snow settling for which we think that the strain leads to

preferentially horizontally oriented ice grains in the snow microstructure. The TGM formulation was validated with existing CT data from laboratory experiments. The strain formulation was calibrated with four years of anisotropy data obtained from polarimetric radar measurements ~~during four winter seasons~~ acquired in Sodankylä, Finland between 2009 and 2013.

~~The results of the model, four years of~~ For calibration, we drove SNOWPACK with meteorological data and used the output to model the depth-resolved anisotropy~~time series, were validated with computer tomographic (CT) measurements of the snow microstructure acquired during four field campaigns. For validation,~~ . Then, we minimized the difference between the depth average of the modeled anisotropy and the depth-averaged radar anisotropy by adjusting a single fit parameter. For sensitivity analysis the fit parameters was determined for each season separately but we determined it also globally for the entire set of all four seasons. Additionally, we run an ensemble of different SNOWPACK configurations to evaluate the model sensitivity to slightly different snowpack properties. We conclude that the same fit parameter can be used for any snowpack because model results improved only marginally when the parameter was adjusted for every season individually. Finally, the modeled, depth-resolved anisotropy profiles were ~~determined from the CT data via exponential correlation lengths p_{ex} derived from two-point correlation functions~~validated with field-measured CT anisotropy profiles. The modeled anisotropy varies between values of ± 0.3 and agrees with the radar data with an root means square error (RMSE) of 0.03 (Pearson-$r = 0.8 \pm 0.2$) and with CT data with an RMSE of less than 0.15 (Pearson-$r = 0.7 \pm 0.2$).

The model results are remarkable in several aspects: ~~First the~~ 1) the model performance allows for improved parametrization of different snow properties like thermal, mechanical and electromagnetic properties. 2) our results indicate a yet undocumented effect of settling on the creation of horizontal structures in new snow. 3) the detailed agreement between the radar-measured anisotropy and the anisotropy modeled ~~solely based on meteorological input~~ from meteorological data demonstrates that polarimetric radar measurements at sufficiently high frequency (10–20 GHz) can be used to monitor the ~~structural~~ evolution of the ~~snow pack. Second, the good agreement~~ structural anisotropy. This has several consequences:

The simplicity of the model allows for immediate implementation into common snow models to simulate the anisotropy, at least during dry snow conditions. We could show with laboratory CT data that for dry snow the growth of vertical structures is proportional to the vertical water vapor flux. Unfortunately, experiments with wet snow metamorphism at the melting point are difficult and only very few studies exist, therefore we could only hypothesize about a formulation for the anisotropy evolution during snow melt which limits our model to dry snow applications.

The observation that the compression of new snow increase horizontal structures could stimulate new laboratory experiments to confirm this mechanism and to study what exactly causes creation of horizontal structures, how different crystal types influence or impede the creation of horizontal structures and how horizontal structures affect the mechanical properties of snow under strain.

The fact, that model, radar measurements and CT data are consistent puts confidence in the interpretation of the radar measured anisotropy. Depending on the system geometry, the anisotropy can be measured only depth-averaged (remote-sensing systems) or even depth-resolved with ~~CT measurements shows that a microstructural parameter like the anisotropy can be modeled solely based on macroscopic fields. Third, the model demonstrates that it can reproduce the~~ in-situ systems as done e.g. for a fast characterization of firn cores (Fujita et al., 2009). Similarly, radar systems mounted on rails could be used to scan the snowpack layer by layer and nondestructively which allows for monitoring of the evolution of the depth-resolved anisotropy. Radar satellites can directly measure the copolar phase difference (CPD) which is proportional to the depth-averaged anisotropy of a dry snowpack. For single radar acquisitions the CPD can be difficult to interpret and can even be zero for a snowpack with equal amounts of layers with positive and negative anisotropies. In contrast, with radar time series, quantitative information e.g. about new snow fall can be obtained because we showed that the transformation by TGM is often slower than the anisotropy ~~which can only be determined with sophisticated CT or radar measurements. Nevertheless, for depth hoar we found that the model significantly underestimates the strong vertical structures which result from CT-data when deriving the anisotropy from p_{ex}~~ increase during accumulation of new snow (Leinss et al., 2014).

Finally, the large observation time spanning four winter seasons with a sampling interval of four hours builds an unique data source to study the evolution of the anisotropy of snow. We think, that the developed model and the determined parameters are relevant for future consideration of the anisotropy in snow models. Beyond that, the ~~well calibrated SNOWPACK model provides an additional~~ SNOWPACK model calibrated with extreme efforts provides a valuable data set to study microwave properties of snow especially within the framework of the Nordic Snow and Radar Experiment (NoSREx-I-III) in Finland, Sodankylä.

With the long time series and the developed model we gained a deeper insight into the anisotropic growth mechanisms of ~~anisotropic snow crystal~~ snow crystals and identified the two main driving terms, the ~~strain rate and the~~ vertical water vapor flux and snow settling. The model could help to enhances the understanding of ~~macroscopic anisotropic properties like thermal conductivity, mechanical~~

~~stability and electromagnetic properties, and~~ the anisotropy of macroscopic snow properties and demonstrates that the anisotropy can be measured by means of polarimetric radar systems ~~which provides a new method~~ to access microstructural properties of snow ~~non-destructive~~ non-destructively and even from space.

7 Data availability

All data are originally from the NoSREx-campaigns (Lemmetyinen et al., 2016, 2013) and are partially available from FMI at www.litdb.fi. Radar data are available from ESA or from the GAMMA Remote Sensing and Consulting AG. Preprocessed meteorological input data, configuration files and simulated snow profiles from SNOWPACK, modeled anisotropy time series, radar-measured anisotropy time series, SWE measurements and CT-data are available under DOI:http://dx.doi.org/10.3929/ethz-b-000334041.

Appendix A: Preprocessing of meteorological data and SNOWPACK calibration

A1 Preprocessing of meteorological data

In order to provide SNOWPACK physically consistent input data all meteorological data were preprocessed, filtered, combined and gaps were interpolated if they could not be filled by data sets of equivalent sensors. Figure S2 shows a processing flow chart of the meteorological data which was used to create the three input files required by SNOWPACK (soillayer*.sno, config*.ini, meteoin*.smet). We combined data measured at the IOA (MAWS*), meteorological mast (arcmast*), and from the AWS. All raw data were downsampled to a 1 hour sampling interval. Invalid data were removed and ~~equivalent~~ redundant datasets were averaged. Data gaps were interpolated with algorithms which considered diurnal and seasonal cycles and also the type and statistics of existing data series~~(details below)~~. For comparison, supplementary figures show raw data (Figs. S3–S6) and processed data (S7–S10).

Snow height (HS) and air temperature (TA) were measured by at least one sensor at each of the three site (IOA, AWS, meteorological mast), but some of the data series contained gaps for periods of a few days. The measurements of the three sensors were very similar (see supplementary figures S3–S6; standard deviation snow height $\sigma_{\mathrm{HS}} = 2.6\,\mathrm{cm}$, max. difference $\Delta\mathrm{HS}_{95\%} < 10\,\mathrm{cm}$ for 95% of measurements. Standard deviation of air temperature $\sigma_{\mathrm{TA}} < 0.6\,\mathrm{K}$, max deviation of air temperature $\Delta T_{95\%} < 2.0\,\mathrm{K}$ for 95% of measurements.). Therefore the data were averaged when data from more than one sensor were available. By this redundancy, we obtained almost complete time series of snow depth and air temperature. Remaining gaps of a few days were interpolated.

Four different soil temperature measurements (TSG) were averaged: they were measured at each two locations 2 cm below the surface few meters apart at the IOA (SMT: soil temp B, soil temp C) and at two sites near the meteorological mast at -5 cm and -10 cm depth. The soil temperature of all four sensors differed less than 1.5 K for 95% of measurements and had a standard deviation of 0.5 K~~(see supplementary figures –)~~.

Soil moisture showed signification variations between the six different sensors (each two sensors at -2 cm and -10 cm depth at the two locations SMT-A and SMT-B at IOA and also two sensors at -5 cm and -10 cm depth at the meteorological mast). However, all sensors showed the same trends with 5–15% $_{\mathrm{vol}}$ liquid water content during summer, 1–3% $_{\mathrm{vol}}$ liquid water content during winter and 15–35% $_{\mathrm{vol}}$ liquid water content during snow melt~~(supplementary figure –)~~.

Relative humidity (RH), wind speed (VW), wind direction(DW), and maximum wind speed (VWM) was only measured at the AWS and gaps of a few days were filled by a combination of linear interpolation, average data from the four seasons and diurnal cycles.

Precipitation (PSUM) was measured 600 m north of the IOA. In order to calibrate the precipitation data to the IOA, we adjusted the precipitation data such that the cumulated precipitation of the AWS ($\mathrm{SWE}_{\mathrm{AWS,cal}}$) follows closely the reference snow water equivalent ($\mathrm{SWE}_{\mathrm{REF}}$), composed by ~~measured SWE data of the SSI and the GWI~~SWE data measured by SnowScat during dry snow conditions and data from the GWI during snow melt (Leinss et al., 2015). Calibration was done by amplifying/decreasing existing precipitation when the cumulated precipitation of the AWS, $\mathrm{SWE}_{\mathrm{AWS,raw}}$, was lower/higher than $\mathrm{SWE}_{\mathrm{REF}}$. A comparison of raw precipitation ($\mathrm{P}_{\mathrm{AWS}}$, blue), calibrated precipitation ($\mathrm{P}_{\mathrm{REF}}$, red) and precipitation change (green) are shown at the top together with the SWE data (below) in Fig. A1. SNOWPACK runs with calibrated and uncalibrated precipitation showed that the calibration of precipitation improved the results for the simulated snow height. Some minor inaccuracies in precipitation data can be detected by comparing measured and modeled snow height, Fig. S**??**.

The precipitation phase (PSUM_PH) was measured by the distrometer located at the IOA (data from www.litdb.fmi.fi). However, the data was not directly used because the distrometer frequently misclassified snow as rain. Therefore, the distrometer data was only used to check the rain/snow threshold (THRESH_RAIN). According to the distrometer data ~~the~~ combined with air temperature data from the AWS we determined a rain/snow threshold ~~is at~~ of $T = 0.73°\mathrm{C}$ or alternatively a linear range from $T_{\mathrm{snow}} = 0.06°\mathrm{C}$ to $T_{\mathrm{rain}} = 1.40°\mathrm{C}$ ~~was obtained~~ (Fig. A2).

A2 calibration and interpolation of radiation data

To provide consistent solar radiation data, data acquired by different sensors between ~~January~~ Jan 2009 and ~~September~~

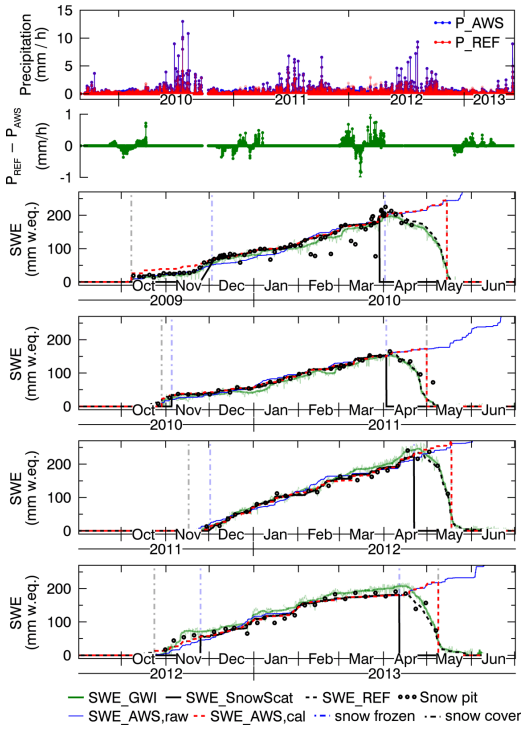

Figure A1. ~~Precipitation and SWE data.~~ Top: precipitation from the AWS~~and~~ , adjusted precipitation (P_{REF}) ~~used to run SNOWPACK. Below in green: Difference between the original~~ and ~~adjusted precipitation data~~difference between both. ~~The four~~ Below, SWE time series ~~below were measured in the~~ derived from different methods are shown: snowpit data (black bullets), ~~by the~~ GWI (green), ~~and by~~ SnowScat (black). Blue and red lines are the cumulated precipitation of the AWS and the adjusted precipitation P_{REF}. Vertical dash-dotted lines indicate ~~the time of~~ snow freeze and melt (light blue) and the period of snow covered ground (gray).~~Snow water equivalent (SWE) was measured by the SnowScat instrument during dry snow conditions. SWE during snow melt was determined by the Gamma Water Instrument (GWI) which was calibrated by manual SWE measurements from the snow pit. To obtain complete time series of SWE (= SWE_{REF}) we composed the SWE signal from GWI measurements (SWE_{GWI}) during wet snow conditions and used radar measurements ($SWE_{SnowScat}$) during dry snow conditions. Details about the SWE measurements with SnowScat, the AWS and the GWI are published in (Leinss et al., 2015).~~

Sep 2015 were homogenized and gaps with missing data were interpolated. Plots of the original raw data and the homogenized and filled data are shown in the supplementary material~~(Supplements,~~ : Fig. S15) ~~.~~

~~Short wave radiation was measured at the sounding station. The short wave sensors were replaced in August 2012, therefore the radiation time series were homogenized to provide consistent time series.Homogenization was done by increasing the reflected radiation by 31% such that the summer albedo was similar before and after sensor replacement.Furthermore, reflected short wave radiation which exceeded incoming short wave radiation was set to 95% of the incoming short wave intensity. Values with reflected short wave radiation of zero were considered as invalid datawhen the incoming radiation exceeded 20 W· m^{-2} . Between 10 November 2011 and 23 March 2012 the reflected short wave sensor malfunctioned. The gap was filled by the product of the~~ (all radiation data), Figs. S3–S6 (seasonal raw data) and Figs. S7–S10 (seasonal filled data). The incoming short wave radiation ~~and the albedo averaged for every day of the year over the period 2009–2015. The albedo at the onset of snow fall (09–19 Nov 2011) was interpolated by manual estimates. Remaining short data gaps in the~~ data was almost complete was interpolated only for a few isolated single days. The reflected short wave radiation data ~~of a few hours were interpolated via the albedo on which an Gaussian average of neighboring pixels was applied (FWHM = 1 day, kernel size = 12 days)~~was modeled by SNOWPACK based on the simulated albedo.

The long wave radiation balance was measured at the radiation tower. Long wave radiation data contained a few gaps up to 20 days long (one gap of 52 days in autumn 2011 is irrelevant because this gap is before the onset of snow fall). Data gaps shorter than 12 days were interpolated by the Gaussian average of neighboring data points (FWHM = 1 day, kernel size = 12 days)~~of neighboring data points~~. Remaining gaps of up to 8 days were linearly interpolated. Additionally, to reconstruct the diurnal radiation cycles, the average radiation of each hour of the year was high-pass filtered (Gaussian window of 6 days) and added to the smoothly interpolated data gaps~~(for plots of the raw and interpolated data see supplementary material, Figs. –, –, and)~~. To provide SNOWPACK the possibility to correctly model

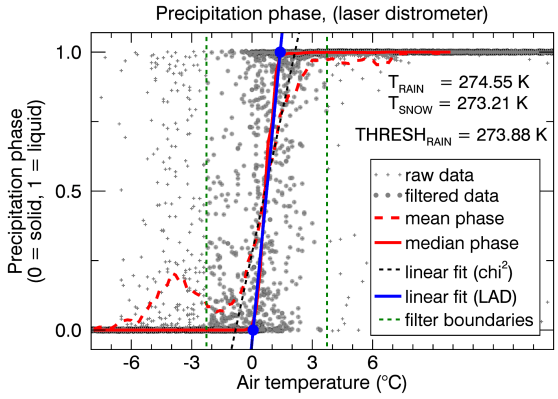

Figure A2. ~~The precipitation phase was measured by the distrometer.~~ From the precipitation phase ~~and the air temperature~~ measured by the ~~AWS~~ distrometer we determined a mean rain/snow threshold of 0.73°C using a robust least-absolute-deviation (LAD) fit ~~to the data~~ (blue line). A linear fit provides the same threshold but a slightly lower slope. Before fitting, we set a filter boundary (green dotted line) of 0.73±3°C. Data outside the ~~filter~~ boundary are considered as misclassified precipitation.

snow melting and settling during the four days 21–23 Nov 2012, the long wave incoming radiation was increased by 45 Wm^{-2} . Webcam observation confirm foggy conditions during this period.

A3 SNOWPACK calibration

For comparison of the natural ~~snow pack~~ snowpack with the modeled ~~snow pack~~ snowpack under different configuration settings, we compared measured and modeled snow height and snow temperature. Snow temperature was measured at five internal snow temperatures sensors at 10, 20, 30, 40, and 50 cm above ground. For snow height and snow temperature we evaluated for each of the four season each six statistical descriptors: the smallest (negative) difference, the largest (positive) difference, the absolute deviation for which 95% of all absolute deviations are smaller, the root mean square error, the mean difference, and the Nash-Sutcliffe model coefficient. Additionally to individual seasons, we calculated these descriptors for the data of all four seasons together. This provided in total ~~60~~ $2 \times (4+1) \times 6 = 60$ quantities for comparisons. To determine the "best" simulation(s), we compared this 60 quantities of every SNOWPACK run with all of the other 5000+ SNOWPACK runs and calculated a score which describes how many times these 60 comparisons show a better result (smaller error, larger Nash-Sutcliffe coefficient) than all other runs. The total score was divided by the total number of runs which results in a score between ~~60 and 0.~~ 0 and 60. A score of 60 indicates that a single run ~~outperfoms~~ outperforms every other run independent ~~on~~ of which statistical variable is analyzed. The maximum achieved score was 51.3, the lowest score 9.3.

Additionally to the relative scoring by pair-wise comparison of all SNOWPACK runs, we used a second scoring scheme which defined fixed height and temperature thresholds for each of the six statistical descriptors. The thresholds are listed in Table A1. The sum of all fulfilled conditions for all years simultaneously and for all individual years made again a maximum score of 60. The score by comparison and score by threshold show an approximately linear relation. Histograms over all SNOWPACK runs with the score by threshold, and the distribution of statistical descriptors are shown in Fig. S18.

For SNOWPACK calibration, we varied the following parameters: scaling of short wave and long wave radiation by various constant factors, various thresholds for the snow/rain threshold (THRESH_RAIN), various factors for the WIND_SCALING_FACTOR with SNOW_EROSION = TRUE/FALSE, five different settings for the ATMOSPHERIC_STABILITY, creation of short wave reflected radiation from albedo (RSWR::create = ISWR_ALBEDO) on/off, Calibrated or uncalibrated precipitation PSUM (see section A1), with or without provided precipitation phase (PSUM_PH in *.smet files), filling of long wave radiation gaps with the generator ILWR::allsky_lw::type = Konzelmann or our method described in section A2, and SW_MODE = BOTH/INCOMING.

Table A1. Thresholds for snow height (HS) and snow temperature (TS) which were used to score the different SNOWPACK runs.

statistical descriptor evaluated for all/each year(s)		threshold value for HS (cm)	threshold value for TS (°C)
smallest negative Difference	>	~~-17~~-10.~~5~~0	~~-9~~-10.~~5~~0
largest positive Difference	<	~~17~~12.~~5~~0	~~14~~10.~~5~~0
max. abs. difference (95%)	<	~~10~~5.0	3.~~4~~0
root mean square error	<	2.5	~~3~~2.~~180~~5
mean difference	<	1.~~6~~0	0.~~29~~20
Nash-Scliffe coefficient	>	0.~~95~~98	0.~~82~~77

We found, that radiation scaling was crucial to produce correct results. Additionally snow erosion with a wind scaling factor around two significantly improved the results. ~~Only with~~ With atmospheric stability = normal ~~, we got good results but the other stability modelswere also not too far from reality~~we got much better results compared to other atmospheric models. Interestingly, only the model MO_MICHLMAYR required not much modification of the radiation in contrast to the other atmospheric models. Setting SW_MODE = INCOMING instead of BOTH did not change the results except near the end of snow melt where a slight change was observable. Obviously, for our test site, SNOWPACK works better when the reflected short wave radiation is estimated via the albedo than vice-versa.

A4 ~~Cost function for determination of α_1 and α_2~~

~~For iterative determination of the free model parameters α_1 and α_2 we defined a cost function which describes approximately the root mean square error between the depth-averaged simulated anisotropy, $A^{\mathrm{mod}}_{\mathrm{avg}}$, and the radar measured anisotropy, $A^{\mathrm{CPD}}_{\mathrm{avg}}$. The cost function is evaluated only for the set M of radar measurements acquired during dry snow conditions. With this set M of about 3200 measurements, where each measurement has the index i , i.e. $i \in M$, we defined the cost function $J(\alpha_1, \alpha_2)$ as~~

$$J(\alpha_1,\alpha_2) = \left[\frac{1}{N}\sum_{i\in M}\left(A^{\mathrm{mod}}_{\mathrm{avg},i} - A^{\mathrm{CPD}}_{\mathrm{avg},i}\right)^2\right]^{1/2} + \left[\frac{1}{N}\sum_{i\in M}\left(A^{\mathrm{mod}}_{\mathrm{avg},i} - A^{\mathrm{CPD}}_{\mathrm{avg},i} - \overline{\Delta A}_{i|i\in M_y}\right)^2\right]^{1/2}.$$

~~In the second term, the subset M_y of M (with $M = \cup_{y=1}^{4} M_y$) defines all radar measurements acquired during an individual winter season y with $y = 1,2,3,4$. In this term, we subtract for each season the mean difference between modeled and measured data. This mean difference, defined by $\overline{\Delta A}_{i|i\in M_y} = \langle A^{\mathrm{mod}}_{\mathrm{avg},i} - A^{\mathrm{CPD}}_{\mathrm{avg},i}\rangle$, where $\langle\cdot\rangle$ indicates the mean, regularizes the cost function as described below.~~

~~Cost functions for the difference between modeled and radar-measured anisotropy used to determine the free model parameters α_1 and α_2 . Shown are the cost-functions for the best SNOWPACK simulation and the entire time range (2009–2013). The cost functions (a): root mean square error (RMS). (b): root mean square error with mean-difference subtracted (RMSc), (c): sum of RMS and RMSc, (d): Nash-Sutteliffe model efficiency coefficient. Cost-functions for individual seasons are provided in the Supplements.~~

~~The regularization is required because the first term in Eq. , evaluated for the range of α_1 , and α_2 , is characterized by an elongated valley structure indicted by contour lines in Fig. ??(a). In this valley, the shallow global minimum is indicated by a white cross. To avoid ambiguities in the shallow minimum of the cost function we added the second term in Eq. which evaluation shows a substantially different structure, Fig. ??(b), than the first term. The different structures originate from the regularization using the mean difference between $A_{\mathrm{avg}}^{\mathrm{mod}}$ and $A_{\mathrm{avg}}^{\mathrm{CPD}}$. This regularization acts as a high pass filter and allows for quantitative consideration of the simulated amplitude of the time-varying anisotropy time series without screening good solutions by seasonally constant (or linearly drifting) offsets. Such offsets can be caused when the anisotropy of the early winter snow pack is not correctly modeled and persists through the entire winter season even though the anisotropy of younger layers accumulated ontop of the early winter layers is correctly modeled. For example, in season 2011/2012, Fig. 7b, the model does not catch the fast growth of vertical structures in Jan/Feb 2012 and an offset exists after February which persists until snow melt. Nevertheless, the amplitude of anisotropy variations between February and April 2012 are quantitatively correctly modeled.~~

~~The error space of the full cost function, comprising both terms of Eq. , is shown in Fig. ??(c). The exploration of the cost function shows that the global minimum can be found with a local hill-climbing optimization method. Because computation of the cost function requires evaluation of all simulated snow layers and time steps a derivation-free algorithm significantly accelerates the optimization. We used the downhill-simplex method (Nelder-Mead or amoeba method). Additionally to the cost function, the model accuracy was measured with the Nash-Sutcliffe model efficiency coefficient which is shown in Fig. ??(d).~~

~~Measured and modeled snow height and SWE (top), and snow temperature at various depths (bottom) for the best SNOWPACK run where snow height was not enforced (ID: optimizeradiation2458414-31824). The gray line in the second-lowest row is equivalent to the soil temperature (TSG, last row) and is helpful to identify unrealistically low measured snow temperatures (e.g. Feb 2011 and possibly Feb 2010 which can be identified very likely as measurement errors). For comparison, blue dots indicate manual snow temperature measurements in a snow pit.~~

~~Measured and modeled snow height, SWE, and snow temperature at various depths for the best SNOWPACK run where snow height was enforced (ID: optimizeradiation2458414-22890). The gray line in the second-lowest row is equivalent to soil temperature (TSG, last row) and can be used to identify unrealistically low measured snow temperatures (e.g. Feb 2011 and possibly Feb 2010 which can be identified very likely as measurement errors). For comparison, blue dots indicate manual snow temperature measurements in a snow pit.~~

Author contributions. SL and HL wrote the manuscript together, SL processed all meteorological and radar data and designed the model, HL processed all CT data, MP, HL and AK collected the field data.

Competing interests. The authors declare that they have no conflict of interest.

Acknowledgements. The *in situ* data collection was supported by the European Space Agency activity "Technical assistance for the deployment of an X- to Ku-band scatterometer during the NoSREx campaigns" (ESA ESTEC Contract no. 22671/09/NL/JA/ef) (Lemmetyinen et al., 2013). The staff at FMI-ARC is acknowledged for the collection of in situ data. Andreas Wiesmann from GAMMA Remote Sensing is acknowledged for technical assistance with the SnowScat data and Margret Matzl for the lab sampling procedures for casted DEP samples. Special thank goes to Jouni Pulliainen from FMI for the initiative of setting up a test site which provides a unique amount and diversity of meteorological data and snow measurements. We thank Matthias Bavey from SLF for helping to find the best SNOWPACK configuration. Juha Lemmetyinen deserve a major thank for his support concerting all details about the test site and the field data. The paper was funded by ETH Zürich. Irena Hajnsek deserves a major thank for ~~her patience and for the freedom~~ providing the space to write this paper.

References

Alley, R. B.: Texture of polar firn for remote sensing, Annals of Glaciology, 9, 1–4, 1987.

Bartelt, P. and Lehning, M.: A physical SNOWPACK model for the Swiss avalanche warning: Part I: numerical model, Cold Regions Science and Technology, 35, 123 – 145, https://doi.org/http://dx.doi.org/10.1016/S0165-232X(02)00074-5, http://www.sciencedirect.com/science/article/pii/S0165232X02000745, 2002.

Brun, E., Martin, E., Simon, V., Gendre, C., and Coleou, C.: An Energy and Mass Model of Snow Cover Suitable for Operational Avalanche Forecasting, Journal of Glaciology, 35, 333–342, https://doi.org/10.3189/S0022143000009254, 1989.

Brun, E., David, P., Sudul, M., and Brunot, G.: A numerical model to simulate snow-cover stratigraphy for operational avalanche forecasting, Journal of Glaciology, 38, 13–22, 1992.

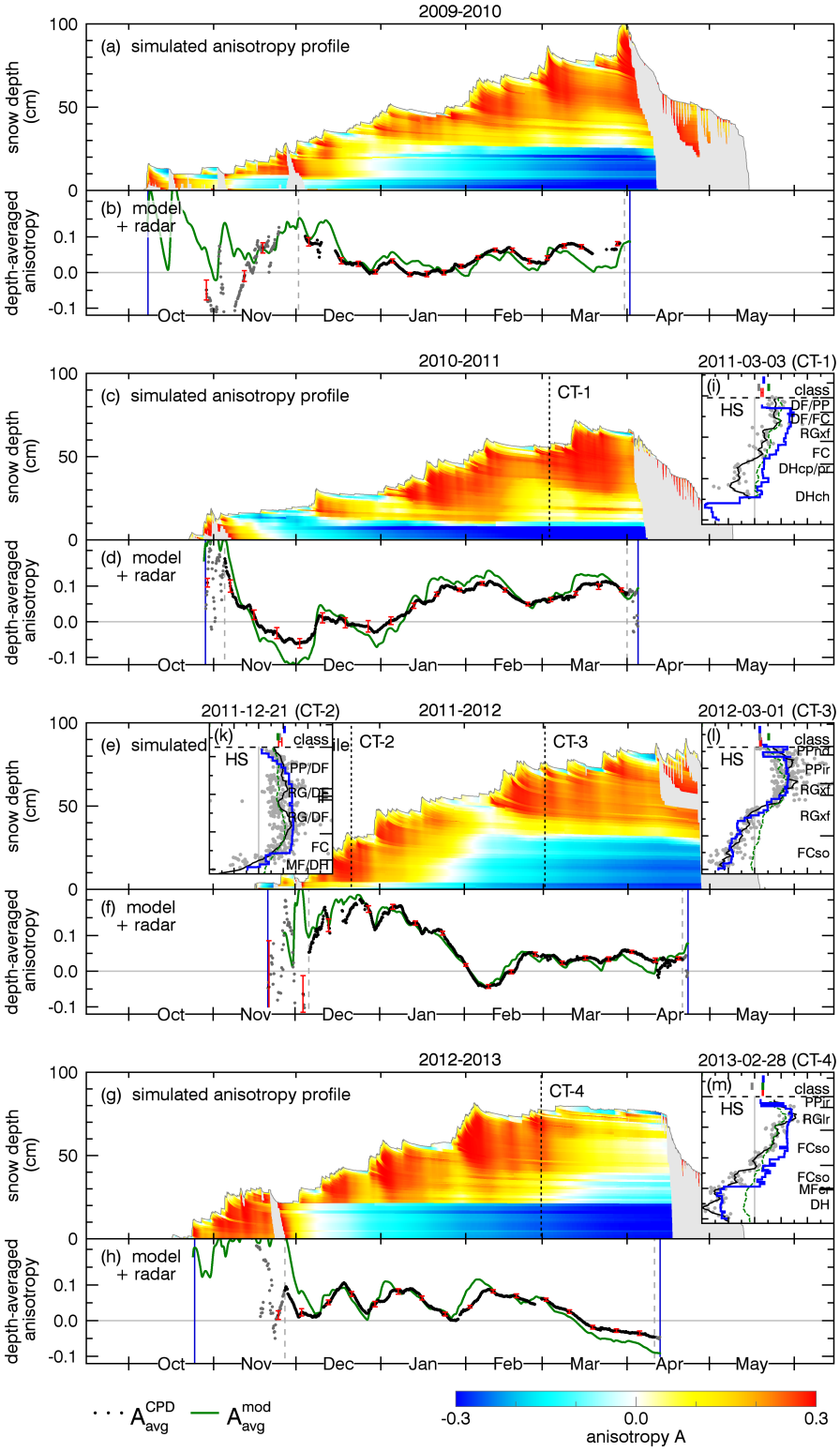

Figure A3. Modeled solution of all four seasons when the ~~parameters α_1 and~~ parameter α_2 ~~are~~ is optimized for ~~the third~~ every season (~~$\alpha_1 = 0.98$ and $\alpha_2 = 0.72$~~ row 1-4, Table 4).

Calonne, N., Flin, F., Morin, S., Lesaffre, B., du Roscoat, Rolland du Roscoat, S., and Geindreau, C.: Numerical and experimental investigations of the effective thermal conductivity of snow, Geophysical Research Letters, 38, 1–6, 2011.

Calonne, N., Geindreau, C., Flin, F., Morin, S., Lesaffre, B., Rolland du Roscoat, S., and Charrier, P.: 3-D image-based numerical computations of snow permeability: links to specific surface area, density, and microstructural anisotropy, The Cryosphere, 6, 939–951, https://doi.org/10.5194/tc-6-939-2012, http://www.the-cryosphere.net/6/939/2012/, 2012.

Calonne, N., Flin, F., Geindreau, C., Lesaffre, B., and Rolland du Roscoat, S.: Study of a temperature gradient metamorphism of snow from 3-D images: time evolution of microstructures, physical properties and their associated anisotropy, The Cryosphere, 8, 2255–2274, https://doi.org/10.5194/tc-8-2255-2014, http://www.the-cryosphere.net/8/2255/2014/, 2014.

Calonne, N., Montagnat, M., Matzl, M., and Schneebeli, M.: The layered evolution of fabric and microstructure of snow at Point Barnola, Central East Antarctica, Earth and Planetary Science Letters, 2016.

Chang, P., Mead, J., Knapp, E., Sadowy, G., Davis, R., and McIntosh, R.: Polarimetric backscatter from fresh and metamorphic snowcover at millimeter wavelengths, IEEE Transactions on Antennas and Propagation, 44, 58 –73, https://doi.org/10.1109/8.477529, 1996.

Colbeck, S. C.: The vapor diffusion coefficient for snow, Water Resources Research, 29, 109–115, https://doi.org/10.1029/92WR02301, http://dx.doi.org/10.1029/92WR02301, 1993.

Davis, R. E. and Dozier, J.: Stereological characterization of dry Alpine snow for microwave remote sensing, Advances in Space Research, 9, 245 – 251, https://doi.org/http://dx.doi.org/10.1016/0273-1177(89)90492-4, http://www.sciencedirect.com/science/article/pii/0273117789904924, 1989.

Fierz, C., Armstrong, R., Durand, Y., Etchevers, P., Greene, E., McClung, D., Nishimura, K., Satyawali, P., and Sokratov, S.: The International Classification for Seasonal Snow on the Ground, 2009.

Fujita, S., Okuyama, J., Hori, A., and Hondoh, T.: Metamorphism of stratified firn at Dome Fuji, Antarctica: A mechanism for local insolation modulation of gas transport conditions during bubble close off, Journal of Geophysical Research: Earth Surface, 114, 1–21, https://doi.org/10.1029/2008JF001143, http://dx.doi.org/10.1029/2008JF001143, 2009.

Heggli, M., Frei, E., and Schneebeli, M.: Instruments and Methods Snow replica method for three-dimensional X-ray microtomographic imaging, Journal of Glaciology, 55, 631–639, https://doi.org/10.3189/002214309789470932, 2009.

Izumi, K. and Huzioka, T.: Studies of metamorphism and thermal conductivity of snow, 1, Low Temperature Science Series A, 33, 91–102, http://eprints.lib.hokudai.ac.jp/dspace/handle/2115/18276, 1975.

Jordan, R.: A one-dimensional temperature model for a snow cover: Technical documentation for SNTHERM. 89., Tech. rep., COLD REGIONS RESEARCH AND ENGINEERING LAB HANOVER NH, 1991.

Kaempfer, T. U., Schneebeli, M., and Sokratov, S. A.: A microstructural approach to model heat transfer in snow, Geophysical Research Letters, 32, n/a–n/a, https://doi.org/10.1029/2005GL023873, http://dx.doi.org/10.1029/2005GL023873, l21503, 2005.

Krol, Q. and Löwe, H.: Relating optical and microwave grain metrics of snow: the relevance of grain shape, The Cryosphere, 10, 2847–2863, https://doi.org/10.5194/tc-10-2847-2016, 2016.

Lamb, D. and Hobbs, P. V.: Growth rates and habits of ice crystals grown from the vapor phase, Journal of the Atmospheric Sciences, 28, 1506–1509, 1971.

Lamb, D. and Scott, W. D.: Linear growth rates of ice crystals grown from the vapor phase, Journal of Crystal Growth, 12, 21 – 31, https://doi.org/https://doi.org/10.1016/0022-0248(72)90333-8, http://www.sciencedirect.com/science/article/pii/0022024872903338, 1972.

Lehning, M., Bartelt, P., Brown, B., and Fierz, C.: A physical SNOWPACK model for the Swiss avalanche warning: Part III: meteorological forcing, thin layer formation and evaluation, Cold Regions Science and Technology, 35, 169 – 184, https://doi.org/http://dx.doi.org/10.1016/S0165-232X(02)00072-1, http://www.sciencedirect.com/science/article/pii/S0165232X02000721, 2002a.

Lehning, M., Bartelt, P., Brown, B., Fierz, C., and Satyawali, P.: A physical SNOWPACK model for the Swiss avalanche warning: Part II. Snow microstructure, Cold Regions Science and Technology, 35, 147 – 167, https://doi.org/http://dx.doi.org/10.1016/S0165-232X(02)00073-3, http://www.sciencedirect.com/science/article/pii/S0165232X02000733, 2002b.

Leinss, S., Parrella, G., and Hajnsek, I.: Snow Height Determination by Polarimetric Phase Differences in X-Band SAR Data, IEEE Journal of Selected Topics in Applied Earth Observations and Remote Sensing, 7, 3794–3810, https://doi.org/10.1109/JSTARS.2014.2323199, 2014.

Leinss, S., Wiesmann, A., Lemmetyinen, J., and Hajnsek, I.: Snow Water Equivalent of Dry Snow measured by Differential Interferometry, IEEE Journal of Selected Topics in Applied Earth Observations and Remote Sensing, 8, 3773 – 3790, https://doi.org/http://dx.doi.org/10.1109/JSTARS.2015.2432031, 2015.

Leinss, S., Löwe, H., Proksch, M., Lemmetyinen, J., Wiesmann, A., and Hajnsek, I.: Anisotropy of Seasonal Snow measured by Polarimetric Phase Differences in Radar Time Series, The Cryosphere, 10, 1–28, https://doi.org/https://doi.org/10.5194/tc-10-1771-2016, 2016.

Lemmetyinen, J., Kontu, A., Leppänen, L., Pulliainen, J., Wiesmann, A., Werner, C., Proksch, M., and Schneebeli, M.: Technical assistance for the deployment of an X- to Ku-band scatterometer during the NoSREx experiment. NoSREx-I, -II and -III (2009 - 2012) Final report. Contract No. 22671/09/NL/JA/ef, Tech. rep., ESA ESTEC, Noordwijk, https://earth.esa.int/web/guest/campaigns, 2013.

Lemmetyinen, J., Kontu, A., Pulliainen, J., Vehviläinen, J., Rautiainen, K., Wiesmann, A., Mätzler, C., Werner, C., Rott, H., Nagler, T., Schneebeli, M., Proksch, M., Schüttemeyer, D., Kern, M., and Davidson, M. W. J.: Nordic Snow Radar Experiment, Geoscientific Instrumentation, Methods and Data Systems, 5, 403–415, https://doi.org/10.5194/gi-5-403-2016, https://www.geosci-instrum-method-data-syst.net/5/403/2016/, 2016.

Leppänen, L., Kontu, A., Vehviläinen, J., Lemmetyinen, J., and Pulliainen, J.: Comparison of traditional and optical grain-size field measurements with SNOWPACK simulations in a taiga snowpack, Journal of Glaciology, 61, 151–162, https://doi.org/10.3189/2015JoG14J026, 2015.

Libbrecht, K. G.: The physics of snow crystals, Reports on progress in physics, 68, 855, 2005.

Löwe, H., Spiegel, J., and Schneebeli, M.: Interfacial and structural relaxations of snow under isothermal conditions, Journal of Glaciology, 57, 499–510, 2011.

Löwe, H., Riche, F., and Schneebeli, M.: A general treatment of snow microstructure exemplified by an improved relation for thermal conductivity, The Cryosphere, 7, 1473–1480, https://doi.org/10.5194/tc-7-1473-2013, http://www.the-cryosphere.net/7/1473/2013/, 2013.

Marti, J. and Mauersberger, K.: A survey and new measurements of ice vapor pressure at temperatures between 170 and 250K, Geophysical Research Letters, 20, 363–366, https://doi.org/10.1029/93GL00105, http://dx.doi.org/10.1029/93GL00105, 1993.

Massman, W.: A review of the molecular diffusivities of H2O, CO2, CH4, CO, O3, SO2, NH3, N2O, NO, and {NO2} in air, {O2} and {N2} near {STP}, Atmospheric Environment, 32, 1111 – 1127, https://doi.org/http://dx.doi.org/10.1016/S1352-2310(97)00391-9, http://www.sciencedirect.com/science/article/pii/S1352231097003919, 1998.

Miller, D. and Adams, E.: A microstructural dry-snow metamorphism model for kinetic crystal growth, Journal of Glaciology, 55, 1003–1011, https://doi.org/doi:10.3189/002214309790794832, http://www.ingentaconnect.com/content/igsoc/jog/2009/00000055/00000194/art00006, 2009.

Mätzler, C.: Applications of the interaction of microwaves with the natural snow cover, Remote Sensing Reviews, 2, 259–387, https://doi.org/10.1080/02757258709532086, 1987.

Mätzler, C.: Autocorrelation functions of granular media with free arrangement of spheres, spherical shells or ellipsoids, Journal of Applied Physics, 81, 1509–1517, https://doi.org/http://dx.doi.org/10.1063/1.363916, http://scitation.aip.org/content/aip/journal/jap/81/3/10.1063/1.363916, 1997.

Mätzler, C.: Relation between grain-size and correlation length of snow, Journal of Glaciology, 48, 461–466, https://doi.org/doi:10.3189/172756502781831287, http://www.ingentaconnect.com/content/igsoc/jog/2002/00000048/00000162/art00011, 2002.

Pinzer, B. R. and Schneebeli, M.: Snow metamorphism under alternating temperature gradients: Morphology and recrystallization in surface snow, Geophysical Research Letters, 36, 1–4, https://doi.org/10.1029/2009GL039618, http://dx.doi.org/10.1029/2009GL039618, 2009.

Pinzer, B. R., Schneebeli, M., and Kaempfer, T. U.: Vapor flux and recrystallization during dry snow metamorphism under a steady temperature gradient as observed by time-lapse micro-tomography, The Cryosphere, 6, 1141–1155, https://doi.org/10.5194/tc-6-1141-2012, http://www.the-cryosphere.net/6/1141/2012/, 2012.

Proksch, M., Löwe, H., and Schneebeli, M.: Density, specific surface area and correlation length of snow measured by high-resolution penetrometry, Journal of Geophysical Research: Earth Surface, 120, 346–362, https://doi.org/10.1002/2014JF003266, 2015.

Rechtsman, M. C. and Torquato, S.: Effective dielectric tensor for electromagnetic wave propagation in random media, Journal of Applied Physics, 103, 084901, https://doi.org/http://dx.doi.org/10.1063/1.2906135, http://scitation.aip.org/content/aip/journal/jap/103/8/10.1063/1.2906135, 2008.

Riche, F. and Schneebeli, M.: Thermal conductivity of snow measured by three independent methods and anisotropy considerations, The Cryosphere, 7, 217–227, https://doi.org/10.5194/tc-7-217-2013, http://www.the-cryosphere.net/7/217/2013/, 2013.

Riche, F., Montagnat, M., and Schneebeli, M.: Evolution of crystal orientation in snow during temperature gradient metamorphism, Journal of Glaciology, 59, 47–55, https://doi.org/doi:10.3189/2013JoG12J116, http://www.ingentaconnect.com/content/igsoc/jog/2013/00000059/00000213/art00005, 2013.

Schleef, S. and Löwe, H.: X-ray microtomography analysis of isothermal densification of new snow under external mechanical stress, Journal of Glaciology, 59, 233–243, https://doi.org/https://doi.org/10.3189/2013JoG12J076, 2013.

Schleef, S., Löwe, H., and Schneebeli, M.: Hot-pressure sintering of low-density snow analyzed by X-ray microtomography and in situ microcompression, Acta Materialia, 71, 185 – 194, https://doi.org/https://doi.org/10.1016/j.actamat.2014.03.004, http://www.sciencedirect.com/science/article/pii/S1359645414001475, 2014.

Schneebeli, M. and Sokratov, S.: Tomography of temperature gradient metamorphism of snow and associated changes in heat conductivity, Hydrological Processes, 18, 3655–3665, https://doi.org/10.1002/hyp.5800, http://dx.doi.org/10.1002/hyp.5800, 2004.

Shertzer, R. H. and Adams, E. E.: Anisotropic thermal conductivity model for dry snow, Cold Regions Science and Technology, 69, 122 – 128, https://doi.org/http://dx.doi.org/10.1016/j.coldregions.2011.09.005, http://www.sciencedirect.com/science/article/pii/S0165232X1100187X, 2011.

Sokratov, S. A. and Maeno, N.: Effective water vapor diffusion coefficient of snow under a temperature gradient, Water Resources Research, 36, 1269–1276, https://doi.org/10.1029/2000WR900014, http://dx.doi.org/10.1029/2000WR900014, 2000.

Srivastava, P. K., Mahajan, P., Satyawali, P. K., and Kumar, V.: Observation of temperature gradient metamorphism in snow by X-ray computed microtomography: measurement of microstructure parameters and simulation of linear elastic properties, Annals of Glaciology, 51, 73–82, 2010.

Srivastava, P. K., Chandel, C., Mahajan, P., and Pankaj, P.: Prediction of anisotropic elastic properties of snow from its microstructure, Cold Regions Science and Technology, 125, 85 – 100, https://doi.org/http://dx.doi.org/10.1016/j.coldregions.2016.02.002, http://www.sciencedirect.com/science/article/pii/S0165232X16300052, 2016.

Staron, P. J., Adams, E. E., and Miller, D. A.: Nonequilibrium thermodynamics of kinetic metamorphism in snow, Cold Regions Science and Technology, 97, 60–71, 2014.

Sturm, M. and Benson, C. S.: Vapor transport, grain growth and depth-hoar development in the subarctic snow, Journal of Glaciology, 43, 42–59, 1997.

Sturm, M., Holmgren, J., König, M., and Morris, K.: The thermal conductivity of seasonal snow, Journal of Glaciology, 43, 26–41, 1997.

Tan, S., Xiong, C., Xu, X., and Tsang, L.: Uniaxial Effective Permittivity of Anisotropic Bicontinuous Random Media Using NMM3D, IEEE Geoscience and Remote Sensing Letters, 13, 1168–1172, https://doi.org/10.1109/LGRS.2016.2574759, 2016.

Theile, T., Löwe, H., Theile, T., and Schneebeli, M.: Simulating creep of snow based on microstructure and the anisotropic deformation of ice, Acta Materialia, 59, 7104 – 7113, https://doi.org/http://dx.doi.org/10.1016/j.actamat.2011.07.065, http://www.sciencedirect.com/science/article/pii/S1359645411005519, 2011.

ToolBox, E.: Thermal Conductivity of common Materials and Gases, https://www.engineeringtoolbox.com/thermal-conductivity-d_429.html, 2003a.

ToolBox, E.: Specific Heat of common Substances, https://www.engineeringtoolbox.com/specific-heat-capacity-d_391.html, 2003b.

Torquato, S.: Random heterogeneous materials, Springer, New York, 2002.

Torquato, S. and Lado, F.: Trapping constant, thermal conductivity, and the microstructure of suspensions of oriented spheroids, The Journal of Chemical Physics, 94, 4453–4462, https://doi.org/http://dx.doi.org/10.1063/1.460635, http://scitation.aip.org/content/aip/journal/jcp/94/6/10.1063/1.460635, 1991.

Vallese, F. and Kong, J. A.: Correlation function studies for snow and ice, Journal of Applied Physics, 52, 4921 –4925, https://doi.org/10.1063/1.329453, 1981.

Vetter, R., Sigg, S., Singer, H. M., Kadau, D., Herrmann, H. J., and Schneebeli, M.: Simulating isothermal aging of snow, EPL (Europhysics Letters), 89, 26 001, http://stacks.iop.org/0295-5075/89/i=2/a=26001, 2010.

Werner, C., Wiesmann, A., Strozzi, T., Schneebeli, M., and Mätzler, C.: The SnowScat ground-based polarimetric scatterometer: Calibration and initial measurements from Davos Switzerland, in: Geoscience and Remote Sensing Symposium (IGARSS), 2010 IEEE International, pp. 2363–2366, https://doi.org/10.1109/IGARSS.2010.5649015, 2010.

Wiese, M. and Schneebeli, M.: Early-stage interaction between settlement and temperature-gradient metamorphism, Journal of Glaciology, 63, 652–662, https://doi.org/10.1017/jog.2017.31, 2017.

Yosida, Z.: Physical Studies on Deposited Snow. I.; Thermal Properties., Contributions from the Institute of Low Temperature Science, 7, 19, 1955.

Zermatten, E., Haussener, S., Schneebeli, M., and Steinfeld, A.: Tomography-based determination of permeability and DupuitForchheimer coefficient of characteristic snow samples, Journal of Glaciology, 57, 811–816, https://doi.org/doi:10.3189/002214311798043799, http://www.ingentaconnect.com/content/igsoc/jog/2011/00000057/00000205/art00004, 2011.